HHS Public Access

Author manuscript

*PET Clin*. Author manuscript; available in PMC 2023 January 01.

Published in final edited form as:

*PET Clin*. 2023 January ; 18(1): 1–20. doi:10.1016/j.cpet.2022.09.001.

# Emerging Role of $^{18}$F-NaF PET/Computed Tomographic Imaging in Osteoporosis:

## A Potential Upgrade to the Osteoporosis Toolbox

**Aaron J. Sheppard, BS**[a], **Sriram S. Paravastu, BS**[a], **Natalia M. Wojnowski, BS**[a,c], **Charles C. Osamor III, BSA**[a], **Faraz Farhadi, BS**[b,d], **Michael T. Collins, MD**[a], **Babak Saboury, MD, MPH**[b,*]

[a]National Institute of Dental and Craniofacial Research, National Institutes of Health, 30 Convent Drive, Building 30, Room 228, Bethesda, MD 20892-4320, USA;

[b]Radiology and Imaging Sciences, Clinical Center, National Institutes of Health, 10 Center Drive, Bethesda, MD 20892-4320, USA;

[c]Northwestern University Feinberg School of Medicine, 420 East Superior Street, Chicago, IL 60611, USA;

[d]Geisel School of Medicine at Dartmouth, 1 Rope Ferry Road, Hanover, NH 03755, USA

**Keywords**

Osteoporosis; Sodium fluoride ($^{18}$F-NaF) PET/CT; Bone mineral density; Bone Turnover; Bone Metabolism

## INTRODUCTION

Osteoporosis is the most common metabolic bone disorder, with an estimated prevalence of 13.1% to 27.1% of women and 3.3% to 5.7% of men over the age of 50 affected.[1,2] As a systemic skeletal disease, osteoporosis results in bone fragility with increased risk for fracture, primarily due to disintegration of the bone microarchitecture leading to a decrease in bone mineral density (BMD) and a loss of trabecular connectivity.[3–5] This deterioration of bone structure is the result of an aberrant bone remodeling process.

Normal bone remodeling consists of the replacement of old bone with new bone through the process of bone resorption and bone formation (by osteoclasts and osteoblasts, respectively). In a healthy adult, the amount of bone resorbed and formed is tightly regulated. From childhood to early adulthood, the rate of bone formation exceeds resorption with BMD peaking in the third decade of life.[2,4,6] After this point, the balance shifts to favor bone resorption, and BMD slowly declines throughout the lifespan of a normal adult, with a period of accelerated bone loss around the time of menopause in women.[6,7] In patients with osteoporosis, the degree of bone resorption is even greater than the degree of formation that takes place during normal aging. Osteoporosis is defined by BMD that is ≤ 2.5 standard deviations below peak bone mass for an age- and sex-matched control group.[5,8]

*Corresponding author. 10 Center Drive, Bethesda, MD 20892. babak.saboury@nih.gov.

## Biological Players in Osteoporosis

Bone mass is the net sum of bone formation and bone resorption. Both arms of the process have been targeted in osteoporosis treatment. Drugs that promote formation (eg, parathyroid hormone analogues) are known as anabolic agents, and those that inhibit resorption are known as antiresorptive agents (eg, denosumab and bisphosphonates).[4,9] Although the cause of osteoporosis can be simply understood by an imbalance between the relative rates of bone formation and resorption, the molecular biology involved is complex. The molecular interactions between osteoprotegerin (OPG), receptor activator of nuclear factor kappa-B ligand (RANKL), and the receptor activator of nuclear factor kappa-B (RANK) are a well-studied aspect of bone remodeling (shown by the bolded arrows in Fig. 1).[5,10,11] RANKL on the surface of osteoprogenitors/osteoblasts binds and activates the osteoclast RANK receptor, which subsequently upregulates nuclear factor kappa-B to kick-start osteoclast differentiation. Osteoblasts also secrete OPG, which acts as a decoy receptor for RANKL and leads to decreased RANKL/RANK interactions.[5] Therefore, the relative levels of OPG and RANKL production contribute to more bone formation or resorption, respectively. Given this relationship, co-opting the interaction between RANKL and RANK (on the osteoclast cell surface) with the drug denosumab, a monoclonal antibody against RANKL that blocks RANKL–RANK interaction, is one of the main weapons in osteoporosis therapy armamentarium.[11,12]

There are many other factors regulating bone formation and remodeling, as summarized in Fig. 1. Briefly, it is recognized that osteocytes also play a key role in regulating bone remodeling and response to mechanical loading. In addition, the osteocyte is increasingly recognized as playing roles in osteoblast and osteoclast function as well as mineral homeostasis, responding to and secreting several factors such as RANKL and FGF23, as shown in Fig. 1.[13,14,16] A major contributor to osteoporosis is the decrease in estrogen seen in postmenopausal women.[17,18] Estrogen has numerous effects on bone remodeling through interactions with the estrogen receptors (ERs). The decline of estrogen has been shown to increase osteoblast apoptosis, increase pro-resorptive cytokines such as interleukin-6 (IL-6), interleukin-1 (IL-1), tumor necrosis factor-α (TNF-α), monocyte colony-stimulating factor, and prostaglandin E2, which act to create an inflammatory environment and increased osteoclastic activity[19] (Fig. 1). Much like the RANKL/RANK interaction, the ERs have been targets for osteoporosis therapy, either through estrogen or estrogen-like molecules including selective ER modifiers that have various actions depending on their activity at certain ER subtypes.[20,21] Several other targets are emerging as potential causes and treatments of osteoporosis, including micro ribonucleic acids (miRNAs), long noncoding RNAs (lncRNA), circular RNAs (cirRNA), reactive oxygen species (ROS), and small molecular inhibitors.[19,22]

As previously mentioned, the normal skeleton peaks in BMD around the third decade and then gradually declines until the end of life.[2,23] This decrease in the bone formation/resorption ratio leads to the gradual decrease in BMD, bone strength, and an increase in fractures. It is also clear that an individual's genetic background plays a major role in both bone mass and bone strength, accounting for up to 50% of the determination of fracture risk[5,24–27] (Fig 2).

Additive to an individual's underlying genetic risk for osteoporosis, are numerous environmental factors including lactose allergies (poor calcium intake), underlying medical conditions predisposing to vitamin D deficiency (gastrointestinal disorders), corticosteroid treatment, chronic inflammation, and nutrient deficiencies have all been shown to affect the biological interactions illustrated by Fig. 1 and linked to osteoporosis.[5,18] The current guidelines to screen women over 65 and men over 70 is merely sufficient to detect an already deteriorated skeleton, and largely misses the biological complexities that come before it.[2,17] Although the current guidelines and tools are largely cost-effective and aid in stratifying patients based on fracture risk, they miss the complex metabolic interactions that may augment the ability to characterize bone health and better manage osteoporosis.[2]

### Impact of Osteoporosis and Current Management

It was estimated that around 12.3 million people in the United States over the age of 50 have osteoporosis, and nearly 30% of individuals who suffer a hip fracture die within 1 year.[28] There is a potential therapeutic window of opportunity to take steps to prevent morbidity from osteoporotic fractures by detecting early changes in bone metabolism. Given the significant degree of morbidity and mortality associated with osteoporotic hip fractures, it is clear that there is a great need for a better predictor for these catastrophic fractures.[29,30] Many clinical groups are recognizing the lack of clinical usefulness in repeated dual-energy X-ray absorptiometry (DXA) scans for the monitoring and prediction of fractures[31–33] In fact, Hillier and colleagues found that 8 years of follow-up DXA scans provided insignificant value to the care of patients with osteoporosis and did not help in predicting future fracture risk any more than the *initial* DXA.[32] It is clear, however, that BMD is a good predictor of long-term fracture risk, especially when combined with other risk factors.[2,9,34] However, the current use of DXA and other structural imaging modalities have poor temporal resolution (predict fracture within a 10 year period), do not allow us to catch bone deterioration early, and miss a lot of heterogeneity that could help to more accurately predict fractures.

As an adjunct to the standard, newer imaging techniques and using radiopharmaceuticals such as $^{18}$F-sodium fluoride ($^{18}$F-NaF) PET/computed tomography (CT) may provide an additional layer of information that could not only aid in detecting changes in bone metabolism and remodeling but also better understand microarchitectural changes in bone.

## CURRENT IMAGING MODALITIES IN OSTEOPOROSIS

This review briefly discusses the current imaging modalities available for screening, diagnosing, and managing osteoporosis. First, we will discuss DXA and newer modalities that assess bone structure. Finally, the authors discuss nuclear medicine technology that allows us to incorporate bone metabolic information with bone architecture. Most importantly, $^{18}$F-NaF PET/CT will be discussed as a powerful tool for assessing skeletal metabolism and health.[35]

## Dual-energy X-ray absorptiometry: Current screening method

Osteoporosis is most commonly evaluated by calculating a patient's BMD using DXA (Fig 3) to find the bone mineral content for a region of interest (ROI).[3] Two different X-ray beams, one low-photon and one high-photon energy, are passed through a ROI (commonly the hip and lumbar spine) to create a pixel-by-pixel map of BMD.[36] The United States Preventive Services Task Force currently recommends all women over the age of 65 years, and men over 70, to be screened for osteoporosis with bone measurement testing via DXA.[37] The diagnosis of osteoporosis is given when a patient's BMD falls into a T-score of −2.5 or lower. Osteopenia, the precursor to osteoporosis, is characterized by a T-score between −1.0 and −2.5. DXA remains a popular modality for clinicians due to the accessibility and low radiation exposure to the patient. A DXA scan only exposes patients to as much radiation as 3 hours of natural background radiation,[38] which is comparable with a musculoskeletal radiograph.[39]

## Quantitative computed tomography: Measuring the density in three-dimension

In the realm of osteoporosis imaging, CT is a more robust modality for analyzing bone cortical and trabecular architecture as well as quantifying BMD. CT can provide information on the three-dimensional (3D) structure of bone, allowing assessment of site-specific differences in structure that may better predict fracture risk.[41] Low-dose scan quantitative CT (qCT) is an imaging modality that relies on standard CT imaging and a phantom representing varying bone mineral concentrations as a standard. As the various mineral content of the phantom is known, the Hounsfield unit (HU) can be calibrated to reflect BMD, providing more accurate measures of BMD compared with using native HUs.[42] There has also been extensive research to develop "phantomless" methods of determining BMD.[43] Although BMD measurements obtained from using phantoms or internal calibration techniques have been shown to have variations from DXA-measured BMD, several groups have shown its effectiveness. A case–control study found that combining phantomless qCT BMD with finite element analysis could predict fractures with an area under the curve (AUC) of 0.692.[44] Another group found that qCT combined with FEA was just as effective as DXA in identifying patients at high risk for fracture.[43,45] Although it is possible to approximate BMD using these methods, it is difficult to precisely measure the BMD (Fig. 4).

## Dual-energy computed tomography: Bone mineral density beyond the basics

Dual-energy CT (DECT) is an X-ray-based technology, similar to DXA, which collects two images at two different X-ray energies and measures tissue-specific attenuation along an X-ray spectrum.[43] The main advantage of the DECT-based BMD measurement is that there is no need for a phantom measurement, or internal calibrations, in order to measure BMD. Similar to DXA, due to the dual spectrum of radiation emitted by the DECT machine, attenuation constants for both of the CT energies can be used to directly calculate the amount of calcium present in bone. Koch and colleagues recently found that DECT-derived BMD values were significantly different from qCT-based measurements and were repeatedly closer to the actual values of hydroxyapatite (HA).[46] Another advantage of DECT over DXA is the ability to see bones in 3D resolution, providing for improved assessment of

the bone architecture. There is a continual advancement of scanners and software packages that can allow a 3D view of BMD. Compared with qCT, DECT shows promise in the diagnosis and management of bone architecture, as well as density disorders without the use of phantoms for BMD approximation. DECT-derived BMD measurements have been recently shown to strongly predict 2-year fracture risk in patients with osteoporosis.[47,48] However, as with all X-ray-based modalities, the information gained from DECT is purely structural and does not convey physiologic information which is crucial to tracking bone disorders over time.

### Metabolic Imaging with $^{18}$F-NaF PET/CT and $^{99m}$T-MDP SPECT/CT

The aforementioned imaging techniques work well for quantifying bone architecture, but as previously mentioned, there is a need for modalities that give insight to bone metabolic activity.

$^{18}$F-NaF is a radiotracer that reflects skeletal metabolism and calcification.[49] It was introduced in 1962 for detection of osteogenic activity,[50] but it was not until the 1990s that NaF regained interest for bone scanning with the global increase in PET and PET/CT.[51] With a half-life of 110 minutes, $^{18}$F-NaF can be injected into the vein and visualized by PET/CT. $^{18}$F-NaF is able to diffuse across membranes and $^{18}$F incorporates into HA (representing bone remodeling) and is rapidly renally cleared.[49] For those reasons, along with the fact that PET scanners have superior resolution to single photon emission computed tomography (SPECT), $^{18}$F-NaF is the preferred radiotracer for bone metabolic activity over the older technetium 99m-methyl diphosphonate ($^{99m}$T-MDP) SPECT/CT.[51–55] $^{18}$F-NaF PET has traditionally been used to detect metastatic bone disease, such as bone metastases from prostate cancer.[56,57] Given its ability to evaluate bone turnover at the molecular level, $^{18}$F-NaF-PET/CT has the potential to provide an alternative superior modality to imaging of metabolic bone disorders to track changes with higher sensitivity.[53]

Furthermore, there are several characteristics of $^{99m}$T-MDP which make it a poor radiotracer for osteoporosis. First, given it is a bisphosphonate, $^{99m}$T-MDP is not rapidly metabolized *in vivo* and relies heavily on renal clearance. This is an issue given renal function steadily declines with age, allowing more of the radiopharmaceutical to enter the bone compartment, thus overestimating osteoblastic activity.[58,59] In addition, $^{99m}$TcMDP binds to plasma proteins, which alters measurements, unlike with $^{18}$F-NaF PET imaging.[51] In addition, the half-life of $^{99}$T-MDP is long compared with $^{18}$F-NaF, at around 6 hours. Thus, the radioactive agent is in the body for longer periods of time and potentially subjecting the subject to greater amounts of radiation.[60]

The remainder of this review expounds on the methodology of $^{18}$F-NaF PET/CT, as well as its ability to give metabolic insight as well as morphologic characteristics, which may aid in screening and managing osteoporosis.

## $^{18}$F-NaF PET/COMPUTED TOMOGRAPHY FOR BONE METABOLIC IMAGING

As alluded to, $^{18}$F-NaF is a reliable measure for assessing bone metabolism. After the sodium and radiolabeled fluoride ions dissociate *in vivo*, the fluoride ion incorporates into

the HA chemical structure as shown by Equation 1.[53] As fluoride can only be incorporated into sites of exposed, newly formed bone mineral, it is a direct measure of osteoblastic activity. However, as osteoblast activity is tightly coupled to osteoclast activity, the amount of $^{18}$F-NaF incorporated into bone mineral is also a strong reflection of osteoclast activity and bone turnover.[51,53]

$$Ca_{10}(PO_4)_6(OH)_2 + 2F^- \rightarrow Ca_{10}(PO_4)_6F_2 + 2OH^- \quad (1)$$

There are two methods for quantifying $^{18}$F-NaF uptake and bone turnover, with each having their own pros, cons, and clinical utility.

## Clinical $^{18}$F-NaF PET and Standardized Uptake Value

The first method, and most widely used in the clinic, entails calculating standardized uptake value (SUV) 60 minutes after radiotracer injection, which reflects $^{18}$F-NaF concentration (kBq/mL) in a ROI normalized to body weight (kg) and injection activity. The SUV is a simple measure of bone turnover, where the SUV can be used as a relative measure of how much newly formed HA is available for the reaction expressed as Equation 1. This can provide useful information about bone metabolic state and bone formation. In the clinic, SUV measurements are routinely used to monitor or detect metastatic bone disease (ie, prostate cancer) and metabolic bone disease.[53,61] Static SUV measurements are advantageous as they allow for shorter scan times, making it more comfortable for the patient and less technically demanding on clinical staff.[61]

While very useful when studying or comparing longitudinal data from focal bone lesions, SUV measurements from $^{18}$F-NaF PET is not the best measure when comparing a population with a systemic bone disorder (ie, osteoporosis and Paget's disease) to a healthy population, as SUV depends on plasma concentration (a point discussed later).[62,63] To get around this dependence on plasma concentrations, more robust, kinetic methods have been developed to better reflect bone metabolism and provide insights into morphologic characteristics Fig. 5.

## Dynamic $^{18}$F-NaF PET and Kinetic Modeling Parameters

By thinking of physiologic and biological systems from the viewpoint of kinetic modeling, there is an opportunity to translate PET images into meaningful physiologic parameters.[49,64,65] The foundation for kinetic modeling, as it relates to bone, comes from thinking about where the $^{18}$F-NaF radiotracer is present from a microanatomical standpoint. Given that NaF freely diffuses across cell membranes and has high tissue extraction (low plasma protein binding), the flow of $^{18}$F-NaF can be modeled by the transfer of radiotracer from the plasma into the bone environment, where there is then exchange between the bone extracellular fluid (ECF) and between the ECF and newly mineralized bone.[35,61] Further, the exchange between the unbound pool of $^{18}$F-NaF and the newly mineralized bone depends on the tightly coupled interactions of osteoblasts, osteoclasts, and osteocytes (see Fig. 1). This exchange of $^{18}$F-NaF within the bone is illustrated in Fig. 6, where the plasma, ECF, and newly mineralized bone compartments are denoted by $C_a$, C1, and C2, respectively.

In the compartment model, the rate of transfer of $^{18}$F-NaF from the arterial compartment to the ECF ($C_a \rightarrow C1$) is denoted by $K_1$, also referred to as the plasma clearance of $^{18}$F-NaF to the ECF, and has units of mL min$^{-1}$ cm$^{-3}$ (*meaning of these parameters discussed later*). The parameters $k_2$ and $k_3$ have units of min$^{-1}$ and represent the rate of transfer from the ECF back to the plasma ($C2 \rightarrow C_a$) and from the ECF to the newly mineralized bone ($C1 \rightarrow C2$), respectively. Although the physiologic meaning of $k_2$ is not immediately clear (discussed later), $k_3$ is a valuable measure of the efficiency of $^{18}$F-NaF uptake into the mineralized compartment. Further, $k_4$ also has units of min$^{-1}$ and represents the backward rate of transfer of $^{18}$F-NaF from the newly mineralized bone compartment to the ECF ($C2 \rightarrow C1$).[66] Finally, it is important to not forget about total bone mineral, as the volume of newly mineralized bone depends on total bone that is available to remodel. This entire model can be simplified into a two-compartment schematic (Fig. 7), commonly referred to as the Hawkins two-compartment bone model.[67]

Now with a working model for the transfer of $^{18}$F-NaF throughout a bone ROI, the law of conservation of matter can be applied to each compartment to obtain the differential Equations 2 and 3.

$$\frac{dC_1}{dt} = K_1 C_a(t) - k_2 C_1(t) - k_3 C_1(t) + k_4 C_2(t) \tag{2}$$

$$\frac{dC_2}{dt} = k_3 C_1(t) - k_4 C_2(t) \tag{3}$$

Here, we have a solvable set of first-order differential equations. The solution to these equations (Equations 4 and 5) is two functions for the concentration of $^{18}$F-NaF over time within the ECF and new bone mineral compartment [$C_1$(t) and $C_2$(t), respectively].

$$C_1(t) = C_a\left[A_{11}e^{-a_1(t)} + A_{12}e^{-a_2 t}\right] \tag{4}$$

$$C_1(t) = C_a A_{22}\left[e^{-a_1(t)} + e^{-a_2 t}\right] \tag{5}$$

Here, Cα is the initial spike in plasma concentration at time zero. $A_{11}$, $A_{12}$, $A_{22}$, $\alpha_1$, and $\alpha_2$ are the algebraic functions of parameters $K_1$, $k_2$, $k_3$, and $k_4$[65].

In PET, we do not know the parameters ($K_1$, $k_2$, $k_3$, or $k_4$). After all, this is the information we are trying to gain from the kinetic model. By measuring the SUVs within a ROI of bone at various time points, we are effectively creating the plot of $C_1(t) + C_2(t)$, which is defined as the tissue activity curve (TAC). $C_a$ can also be plotted by measuring the SUV within an arterial ROI (ideally the artery that supplies the bone ROI) over a period of time. This is defined as the arterial input function (AIF). With knowledge of our kinetic model, computational methods and regression algorithms can be applied to the TAC and AIF to estimate the parameter values that best fit the compartmental model.

Hawkins and colleagues proposed a method to measure plasma clearance of $^{18}$F-NaF using 60-min dynamic $^{18}$F-NaF PET scans, which are performed by acquiring multiple scans with increasing time frames over the protocol duration.[67] This method uses a nonlinear regression using the two-compartment kinetic model (described up to this point) to estimate the four rate constants to describe the movement of $^{18}$F-NaF between the compartments. The kinetic parameters can provide insightful bone physiology measures (Table 1).

**$K_1$—**Since the extraction efficiency of $^{18}$F-NaF into the bone compartment from the arterial compartment is nearly 100%, the value of $K_1$ is a good estimate of bone perfusion and has been shown to be in agreement with $^{15}$O-$H_2O$ studies (the gold standard for blood flow studies).[66,68]

This perfusion parameter may be very useful in terms of osteoporosis, as bone perfusion is crucial to maintaining skeletal health.[69,70,77] Going back to osteoblast and osteoclast coupling, it is reasonable to conclude that decreased blood supply, and subsequent increase in catabolic molecules that may contribute to the increase in osteoclast activity. This is supported by studies that find low bone perfusion is correlated with greater bone loss and increased fracture risk.[71,78] It is also important to consider the ROI with higher blood flow. When blood flow is high, there is insufficient time for the $^{18}$F-NaF to equilibrate with the tissue, thus $K_1$ can underestimate true bone perfusion in this case. This is illustrated by the findings that $K_1$ is lower than expected in the lumbar spine, a tissue ROI that is highly metabolically active.[66,72] Therefore, $K_1$ can potentially give an extra layer of useful information about bone perfusion or a data point to better normalize other parameter measurements.

**$K_i$—**$K_i$ is the most widely used and reported parameter and is calculated from Equation 6. Given the units of $k_3/(k_2+k_3)$ cancel, $K_i$ has the same units as $K_1$ of mL min$^{-1}$ mL$^{-1}$.

$$K_i = K_1\left(\frac{k_3}{k_2 + k_3}\right) \tag{6}$$

$K_i$ is also referred to as the net plasma clearance of $^{18}$F-NaF from the plasma to bone mineral.[66,79] Another way of thinking about $K_i$ is that it is the volume of plasma cleared of $^{18}$F-NaF per mL of bone per minute. This parameter is also widely referred to as a measure of bone turnover and bone metabolic flux.[79,80] Several groups have shown $K_i$ positively correlated with bone histomorphometric data of bone turnover, such as osteoblast per bone area, osteoclast per bone area, and bone formation rate (BFR), with $r^2$ values between +0.49 and +0.63.[74,75] Given that $K_i$ is associated with both osteoblast and osteoclast activity, this parameter is best described as a measure of the coupling of bone remodeling processes and does not necessarily inform about the direction of bone formation, which depends on the relative rates of osteoblast and osteoclast activity. Therefore, calling $K_i$ bone metabolic flux can be misleading since it does not tell you whether the mineral flux is positive or negative.

**$k_2$, $k_3$, and $k_4$—**In the two-compartment model, $k_3$ is the transfer of $^{18}$F-NaF from the unbound ECF to the newly mineralized bone. $k_3$ may be the most direct measure of

mineralization rate and osteoblast activity as it represents the transfer rate of tracer from the ECF to bone without the influence of other parameters. In a study of teriparatide treatment, only $k_3$ showed a significant increase, where no change was observed in $K_1$, $k_2$, and $k_4$, indicating $k_3$ was a sensitive measure of increased osteoblast function.[49] The true usefulness behind $k_2$ and $k_4$ is not fully understood. In Paget's disease, Cook and colleagues found that as $k_3$ increased, $k_2$ decreased, reflecting the increased bone turnover.[76] Also, it is thought $k_2$ may provide insight into bone morphology. For example, Paget's disease is accompanied by less marrow space (due to increased bone volume and crowding of trabecular space), and therefore the decrease in $k_2$ may be explained by the fact that it is more difficult for the tracer to return to the blood pool.[72,76] $k_4$ is the rate of $^{18}$F-NaF flow from the new bone mineral to the ECF. Although many groups neglect this parameter due to its near zero value, others have shown that $k_4$ may provide important data when assessing overall kinetics.[81–83] The non-zero value for $k_4$ suggests that there is a small fraction of $^{18}$F-NaF that is weakly bound to HA, and one study found that neglecting this value results in underestimation of $K_i$.[66]

**$K_1/k_2$ as a measure of extracellular fluid volume—**The ratio of $K_1/k_2$ has been proposed as a measure of the volume of distribution of $^{18}$F-NaF within the ECF compartment. Assuming passive diffusion of fluoride between plasma and ECF, $K_1/k_2$ would represent the volume of total bone ROI occupied by ECF. However, this is not a great assumption, as fluoride is a small negatively charged molecule and is known to bind hydrogen to create HF, which can cross cell membranes.[66] Several groups have shown that $K_1/k_2$ is positively correlated with the amount of marrow space (ie, lumbar vertebrae trabecula displays higher relative $K_1/k_2$ than humoral bone).[72,84] In one study, Puri and colleagues argues that the reason $K_i$ values at the hip were three-fold lower compared with the lumbar spine is due to the increase in $K_1/k_2$ seen at the spine. They found that there were significantly greater $K_1/k_2$ ratios at the lumbar vertebrae, suggesting more functioning red marrow and relatively greater levels of $^{18}$F-NaF within the ECF.[83]

Interestingly, $K_1/k_2$ may also give some insight into the composition of the bone marrow.[66,69] For example, higher levels of marrow fat is negatively correlated with bone perfusion, as fat replaces healthy red marrow and decreases the effective trabecular ECF space. Thus, higher amounts of marrow fat would result in lower $K_1/k_2$ ratios. Given bone marrow fat is correlated with age and osteoporosis, this could be yet another important parameter, or means for making sense of other measures such as $K_i$ or SUVs of osteoporosis patients.[85]

## A Simpler Method: Patlak Plot

One of the drawbacks of the Hawkins method is it requires complex computational methods. However, by assuming $k_4$ is negligible, and $^{18}$F-NaF is irreversibly bound to the mineral compartment, the model can be simplified.[86,87] The mathematics simplify, allowing the clearance of $^{18}$F-NaF to the bone mineral compartment ($K_i$) to be determined by a graphical approach. To do this, the measured positron emission tomography (PET) activity within the tissue ROI is divided by the plasma activity and plotted as a function of normalized

time, which is the integral of the input curve from initial time of injection divided by the instantaneous plasma concentration.[65,81] The slope of this plot is equal to $K_i$ (Fig. 8).

This simplified approach is widely used as a measure of $K_i$, and several groups have shown that $K_i$ from the Patlak method is highly correlated with $K_i$ obtained with the Hawkins method.[86–91]

### Making Sense of the Methods

It is important to call attention to the differences between the values obtained from SUVs, Patlak $K_i$, and Hawkins $K_i$.

Several groups have found that there is no obvious correlation between SUV measurements and age.[92,93] In fact, Kurata and colleagues found that the SUVmax in the humeral shaft was positively correlated with advanced age, but the SUVmax in the lumbar spine was negatively correlated with age.[92] It is likely that these differences are due to several factors, such as differences in regional blood flow and bone microarchitecture, in which case kinetic data could provide the most insight.[83,94] In addition, Blake and colleagues point out a potential limitation of SUV measurement being the fact that a finite amount of radiotracer must be distributed to bone throughout the body.[49] So, in systemic metabolic diseases such as Paget's disease and osteoporosis, there are multiple sites throughout the skeleton that are competing for $^{18}$F-NaF, which competes for radiotracer.[49,95] Therefore, the SUV measurement may be underestimated at other sites throughout the skeleton.[49,62] To illustrate this point, a study of osteoporotic patients treated with teriparatide for 6 months found that the total plasma concentration of $^{18}$F-NaF decreased by 21%, resulting in minimal change in SUV (3%). However, the $K_i$ obtained from the dynamic scan saw a significant 24% increase.[62] Therefore, the kinetic analysis, if done meticulously, can remove the confounding influence of plasma concentration and provide perfusion status that can improve the conclusions made on analysis of $^{18}$F-NaF PET data.

In a recent meta-analysis by Assiri and colleagues, it was found that the Patlak method had the lowest precision error and allowed for fewer study participants to show a significant treatment response.[87] $K_i$ determined from the Hawkins method showed the highest precision error, which is explained by the high precision errors of each individual parameter (around 30% or greater each).[66] It can be reasoned that the Patlak method has the best sensitivity for clinical practice and research, but it can be argued that the variability of the other parameters ($K_1$, $k_2$, $k_3$, $k_4$, and so forth) can explain intersubject differences in bone characteristics that may be useful in predicting, or characterizing, bone health. Even with the Hawkins method, $K_i$ has the least precision error of the parameters and is the most widely reported parameter to describe bone metabolism.[35]

## $^{18}$F-NaF PET/COMPUTED TOMOGRAPHY AS AN ADJUNCT FOR SCREENING AND MONITORING OSTEOPOROSIS

To this point, we have reviewed the established methods of measuring bone turnover using $^{18}$F-NaF PET/CT. The aim being to deliver an overall understanding of how each method works, the insight that may come from the parameters as it relates to bone health, and

the important considerations and nuances. This section presents the current evidence for why $^{18}$F-NaF PET/CT may serve as a valuable upgrade to the available tools for managing osteoporosis.

A retrospective study of 139 patients (from CAMONA cohort) calculated a bone metabolism score (BMS) using $^{18}$F-NaF-PET/CT. To do this, the authors segmented the entire femoral neck, and then created a subsegment only capturing the cortical and trabecular bone. The SUV within the segmented bone region was normalized by dividing it by the SUV of the entire femoral neck to create the BMS. They found that women over the age of 50 had a significantly lower BMS. Further, they noticed that patients who were classified as osteopenic ($-1 < T < -2.5$) had a wide spread of BMS, suggesting $^{18}$F-NaF-PET/CT may be a valuable adjunct to DXA to provide insight into bone metabolism in the femoral neck and be useful for assessing fracture risk in patients where bone mineral density (BMD) provides inconclusive risk determination.[96] These findings echo other studies showing decreased SUV and $K_i$ in osteoporosis patients[35] (Fig. 9).

However, should there be a decrease in $^{18}$NaF PET signal in osteoporosis? After menopause, biological bone turnover markers (osteoclast markers) are *increased* by 90%, whereas bone formation markers are only *increased* by 45%.[5,97] As there is increased overall bone turnover and bone formation (just resorption outruns formation), one would expect an increased $^{18}$F-NaF PET signal. However, the opposite is generally seen. To understand this, one must consider the resolution of PET/CT imaging. For standard CT scans done in clinical practice, the voxel size is around 2 mm$^3$, where the average trabecular thickness is 50 to 400 μm.[98] Thus, the signal detected by PET is the summation of bone turnover occurring within many bone remodeling units throughout the trabeculae. If the number of trabeculae decreased significantly and the metabolic activity did not change (amount of osteoclast–osteoblast activity per remodeling unit), then the signal would be decreased as there are less remodeling units per voxel. In another example more similar to osteoporosis (Fig. 10), there can be greater bone turnover per remodeling unit, but because there are less trabecular (less bone surface area for bone remodeling units), the signal on $^{18}$F-NaF PET can be less per voxel.

Given that $^{18}$F-NaF PET data are affected by bone microarchitecture, it is difficult to compare the bone turnover data across populations with different bone morphology. There is a great need for further research to better understand how bone morphology affects $^{18}$F-NaF PET/CT data, so that it can be compared with healthy individuals. As mentioned, menopause is a major factor for developing osteoporosis. With the average age of menopause occurring at age 51 and the recommended screening age being 65, there is a potential 14-year window of metabolic change that is largely unmonitored leading up to the development of osteoporosis. Presumably, if an individual is in the early stages of osteoporosis (when bone microstructure is still normal relative to age-matched controls), $^{18}$F-NaF PET would show an increase in signal reflecting the increase in bone turnover (SUV and $K_i$). However, once microstructure declines, the $^{18}$F-NaF PET signal also declines, even though it is possible that there is an increase in bone turnover. If $^{18}$F-NaF PET data can be adjusted by bone architecture in the future, then it is possible that we will be capable of accurately monitoring

relative bone turnover, which will improve monitoring disease progression and fracture risk prediction.[1,23,99]

The major outcome that clinicians aim to prevent in a patient with osteoporosis is bone fracture; however, many patients who sustain fractures do not meet the BMD T-score criteria for osteoporosis.[100–104] As previously alluded to, *repeat* DXA scans provide little to no added benefit when assessing future fracture risk in patients with osteoporosis.[32] It is increasingly recognized that bone turnover markers, such as alkaline phosphatase (ALP), osteocalcin (OC), and carboxy terminal cross-linked telopeptide of type I collagen (CTX), are increased in people with high fracture risk.[105–109] In a prospective cohort of 435 women, subjects who had ALP and CTX levels in the highest quartile had a 2-fold increase in fractures, with relative risks of 2.4 and 2.3, respectively. Interestingly, Messa and colleagues has shown that the $K_i$ from dynamic $^{18}$F-NaF PET is significantly correlated with global bone turnover markers ALP and parathyroid hormone (PTH) of patients with renal osteodystrophy ($r^2 = 0.81$ and $r^2 = 0.93$, respectively).[110] These markers only give a measure of global bone turnover, where $^{18}$F-NaF PET/CT adds the ability to measure bone turnover at site-specific locations with higher sensitivity which correlates with histomorphometric data.[52,74,110] In their study of 26 patients with end-stage renal disease and suspected renal osteodystrophy, Aaltonen and colleagues showed that $K_i$ was significantly correlated with histomorphometric measures such as osteoblast per bone surface (OB/BS) ($r^2 = 0.49$), osteoclasts per bone surface (OC/BS) ($r^2 = 0.62$), BFR ($r^2 = 0.63$), and erosion surface per bone surface (ES/BS) ($r^2 = 0.57$).[74] Additional studies report an even higher correlation between $K_i$ and BFR ($r^2 = 0.71$ and $r^2 = 0.65$).[110,111] Aaltonen and colleagues went on to show that $K_i$ from $^{18}$F-NaF PET alone was able to differentiate patients with low turnover versus non-low turnover (defined by histomorphometric analysis) with a sensitivity of 76% and specificity 78% with an AUC of 0.82.[74] It is important to note, these experiments were carried out on bone from the same disease state and likely similar microstructure. Thus, if $^{18}$F-NaF PET data can be adjusted by bone microarchitecture, then it has the potential to be a powerful tool to noninvasively assess bone metabolism and potentially catch abnormal bone metabolism before it leads to structural change.

Further, there is a great need for future studies to investigate the added value of dynamic $^{18}$F-NaF-PET/CT and kinetic parameters in fracture risk prediction. It is likely that the kinetic parameters ($K_1$, $k_2$, $k_3$, $k_4$, $K_i$, and $K_1/k_2$) may provide added information that can more reliably and accurately characterize bone status and fracture risk. From our literature review, there are no studies that integrate these parameters as a tool for characterizing bone in a way to predict bone fractures or predict structural change.

## Monitoring Response to Treatment

One of the most promising applications for $^{18}$F-NaF PET is monitoring response to therapy for osteoporotic patients. As structural changes of bone can take years to improve or decline with treatment, there is a need for an imaging technique with better sensitivity and temporal resolution to monitor response to treatment[112,113]

First-line treatment for osteoporosis is antiresorptive therapy with bisphosphonates that bind to HA binding sites on bone, stimulating apoptosis of osteoclasts and thereby inhibiting

bone resorption. A study of 24 postmenopausal women with glucocorticoid-induced osteoporosis examined the effect of treatment with alendronate, a bisphosphonate, on bone metabolism via $^{18}$F-fluoride, demonstrated significant decreases in bone metabolism and turnover in the lumbar spine.[114] These metabolic changes are observed in $^{18}$F-NaF PET before changes in ALP and BMD. In fact, SUV at the lumbar spine significantly decreased as early as 3 months, whereas ALP did not significantly change until 6 months, and BMD did not increase until 12 months.[114] Further, a study of 18 women with T-scores less than −2 treated with risedronate found similar findings to the prior study with $K_i$, net plasma clearance to bone mineral displaying a significant decrease as soon as 6 months of treatment on $^{18}$F-fluoride PET.[94] To further illustrate the added sensitivity of dynamic $^{18}$F-NaF PET/CT, this group also found that $K_1$ was not significantly affected by risedronate, whereas $k_3/k_2 1 k_3$ decreased by 18%.[115] This finding suggests the major effect of treatment was on the available sites for radiotracer disposition, clearly showing a decrease in osteoblast activity. It is clear that dynamic $^{18}$F-NaF PET parameters can provide valuable measures to more accurately assess the desired treatment response of a therapeutic.

Studies have also been done to monitor response to treatment with teriparatide, a synthetic PTH analog that works by activating both osteoblasts and osteoclasts, with preferential activation of osteoblasts. Frost and colleagues randomized 27 osteopenic females ($-1 < T < -2.5$) into two groups, where one received calcium and vitamin D and the other received teriparatide along with calcium and vitamin D. They then performed 60-min dynamic $^{18}$F-NaF PET scans at baseline and 12 months after treatment. They found that the teriparatide group had a significant increase in $K_i$ at all ROIs analyzed, including the hip, lumbar spine, femoral shaft, and femoral shaft trabecular.[63] Interestingly, this same study performed DXA scans on the patients and found that BMD significantly increased at the lumbar spine, but only modestly increased at the hip and did not increase at the femoral neck ROI. This finding parallels the findings from clinical trials where teriparatide was shown to have the greatest increase in BMD at the lumbar spine and not significantly affect BMD at the hip.[116–118] By investigating further, other groups found that teriparatide actually decreased cortical density by increasing turnover within the cortical region of the femoral neck while at the same time increasing trabecular volume. Thus, DXA was unable to measure a difference in BMD due to these opposing effects, despite great overall bone anabolic activity.[116] On mechanical testing, the mechanical strength of the femoral neck ROI increased; however, this increase in biomechanical strength was only observed at either 18 or 24 months.[116,117] Therefore, these findings suggest that teriparatide effect on bone structure can take up to 2 years, where the study by Frost and colleagues was able to report a significant increase in bone anabolic activity as early as 12 months. This further supports the ability of $^{18}$F-NaF PET to predict future bone structure and architecture, suggesting it is the optimal biomarker for observing treatment response to teriparatide.

## SUMMARY

Osteoporosis is a metabolic bone disorder characterized by a dysregulation of osteoblast, osteoclasts, and osteocytes that leads to a fragile skeleton. The current standard of characterizing osteoporosis by bone density and structural architecture at particular ROIs is incapable of capturing this complex bone biology. These structural approaches (namely

DXA) have their pitfalls in reliably predicting fractures. Patients with the same T-score have different rates of fracture, and fractures in non-hip and non-vertebral bones are collectively more common in osteoporotic patients.[119] This is concerning and highlights the need for a more sensitive imaging modality to better assess and categorize patients for fracture risk. $^{18}$F-NaF-PET is a promising imaging modality for early detection and monitoring of metabolic bone disorders that alter bone biology. $^{18}$F-NaF-PET can be used as a tool to assess bone turnover and aid in characterizing bone morphology, as well as a tool to monitor response to treatment. Here, we have laid out the various methods of $^{18}$F-NaF PET/CT for assessing bone turnover. Although they each have their limitations, SUV measurements from a static $^{18}$F-NaF PET/CT scan is likely the easiest and most clinically applicable method to capture bone turnover throughout the skeleton. These static scans can sensitively assess longitudinal progression of bone metabolism and treatment response. Dynamic $^{18}$F-NaF PET/CT and kinetic parameter estimation is a more technically challenging technique but may provide more useful research data, including estimates of bone perfusion, insights into ECF space volume, and osteoblast activity. Even more powerful is the fact that all kinetic parameters can be measured voxel-by-voxel within a larger ROI such as the femoral neck. This high-resolution mapping of bone turnover has great potential by not only the ability to reconstruct a 3D view of bone turnover but also assess treatment response, which may have spatial heterogeneity. Further research must continue to explore ways to refine kinetic $^{18}$F-NaF PET/CT data in a way that is clinically useful and comparable across heterogeneous populations. Nevertheless, $^{18}$F-NaF PET/CT may prove to be a much needed upgrade to the osteoporosis toolbox in the near future.

## DISCLOSURE

This research was supported by the Intramural Research Program of the NIH Clinical Center and National Institute of Dental and Craniofacial Research. The opinions expressed in this publication are the author's own and do not reflect the view of the National Institutes of Health, the Department of Health and Human Services, or the United States government. This work was also made possible by the NIH Medical Research Scholars Program, which is a public-private partnership supported jointly by the NIH and generous contributions to the Foundation for the NIH from the Doris Duke Charitable Foundation, the American Association for Dental Research, the Colgate-Palmolive Company, alumni of student research programs, and other individual supporters via contributions to the Foundation for the National Institutes of Health.

## REFERENCES

1. Sarafrazi N. Osteoporosis or low bone mass in older adults: United States, 2017–2018. Centers Dis Control Prev 2021. 10.15620/cdc:103477.
2. Viswanathan M, Reddy S, Berkman N, et al. Screening to prevent osteoporotic fractures: Updated evidence report and Systematic review for the US preventive Services Task Force. JAMA 2018;319(24):2532–51. [PubMed: 29946734]
3. Compston JE, McClung MR, Leslie WD. Osteoporos Lancet 2019;393(10169):364–76. [PubMed: 30696576]
4. Barnsley J, Buckland G, Chan PE, et al. Pathophysiology and treatment of osteoporosis: challenges for clinical practice in older people. Aging Clin Exp Res 2021;33(4):759–73. [PubMed: 33742387]
5. Eastell R, O'Neill TW, Hofbauer LC, et al. Postmenopausal osteoporosis. Nat Rev Dis Primers 2016;2: 16069. [PubMed: 27681935]
6. Berger C, Langsetmo L, Joseph L, et al. Change in bone mineral density as a function of age in women and men and association with the use of antiresorptive agents. CMAJ 2008;178(13):1660–8. [PubMed: 18559803]

7. Lindgren E, Karlsson MK, Lorentzon M, et al. Bone traits Seem to develop also during the third decade in life-normative cross-Sectional data on 1083 men aged 18–28 years. J Clin Densitom 2017;20(1): 32–43. [PubMed: 27546559]
8. World Health Organization. Assessment of fracture risk and its application to screening for postmenopausal osteoporosis : report of a WHO study group [meeting held in rome from 22 to 25 june 1992]. World Health Organization; 1994. Available at: https://apps.who.int/iris/handle/10665/39142. Accessed August 19, 2022.
9. Kanis JA, Cooper C, Rizzoli R, et al. Scientific advisory board of the European Society for clinical and economic aspects of osteoporosis (ESCEO) and the committees of Scientific advisors and national Societies of the international osteoporosis foundation (IOF). European guidance for the diagnosis and management of osteoporosis in postmenopausal women. Osteoporos Int 2019;30(1): 3–44. [PubMed: 30324412]
10. Eriksen EF. Cellular mechanisms of bone remodeling. Rev Endocr Metab Disord 2010;11(4): 219–27. [PubMed: 21188536]
11. Kong YY, Yoshida H, Sarosi I, et al. OPGL is a key regulator of osteoclastogenesis, lymphocyte development and lymph-node organogenesis. Nature 1999;397(6717):315–23. [PubMed: 9950424]
12. Matsumoto T, Endo I. RANKL as a target for the treatment of osteoporosis. J Bone Miner Metab 2021;39(1):91–105. [PubMed: 33057808]
13. Han Y, You X, Xing W, et al. Paracrine and endocrine actions of bone-the functions of secretory proteins from osteoblasts, osteocytes, and osteoclasts. Bone Res 2018;6:16. [PubMed: 29844945]
14. Guo YC, Yuan Q. Fibroblast growth factor 23 and bone mineralisation. Int J Oral Sci 2015;7(1):8–13. [PubMed: 25655009]
15. Eastell R, Szulc P. Use of bone turnover markers in postmenopausal osteoporosis. Lancet Diabetes Endocrinol 2017;5(11):908–23. [PubMed: 28689768]
16. Bolamperti S, Villa I, Rubinacci A. Bone remodeling: an operational process ensuring survival and bone mechanical competence. Bone Res 2022; 10(1):48. [PubMed: 35851054]
17. Arceo-Mendoza RM, Camacho PM. Postmenopausal osteoporosis: latest guidelines. Endocrinol Metab Clin North Am 2021;50(2):167–78. [PubMed: 34023036]
18. Armas LAG, Recker RR. Pathophysiology of osteoporosis: new mechanistic insights. Endocrinol Metab Clin North Am 2012;41(3):475–86. [PubMed: 22877425]
19. Gao Y, Patil S, Jia J. The development of molecular biology of osteoporosis. Int J Mol Sci 2021;22(15). 10.3390/ijms22158182.
20. Ettinger B, Black DM, Mitlak BH, et al. Reduction of vertebral fracture risk in postmenopausal women with osteoporosis treated with raloxifene: results from a 3-year randomized clinical trial. Multiple Outcomes of Raloxifene Evaluation (MORE) Investigators. JAMA 1999;282(7):637–45. [PubMed: 10517716]
21. Noh JY, Yang Y, Jung H. Molecular mechanisms and emerging therapeutics for osteoporosis. Int J Mol Sci 2020;21(20). 10.3390/ijms21207623.
22. Yang Y, Yujiao W, Fang W, et al. The roles of miRNA, lncRNA and circRNA in the development of osteoporosis. Biol Res 2020;53(1):40. [PubMed: 32938500]
23. Demontiero O, Vidal C, Duque G. Aging and bone loss: new insights for the clinician. Ther Adv Musculoskelet Dis 2012;4(2):61–76. [PubMed: 22870496]
24. Xu Y, Ma J, Xu G, et al. Recent advances in the epigenetics of bone metabolism. J Bone Miner Metab 2021;39(6):914–24. [PubMed: 34250565]
25. Ralston SH, Uitterlinden AG. Genetics of osteoporosis. Endocr Rev 2010;31(5):629–62. [PubMed: 20431112]
26. Zhu X, Bai W, Zheng H. Twelve years of GWAS discoveries for osteoporosis and related traits: advances, challenges and applications. Bone Res 2021;9(1):23. [PubMed: 33927194]
27. Rozenberg S, Bruyère O, Bergmann P, et al. How to manage osteoporosis before the age of 50. Maturitas 2020;138:14–25. [PubMed: 32631584]
28. Curry SJ, Krist AH, Owens DK, et al. , US Preventive Services Task Force. Screening for osteoporosis to prevent fractures: US preventive Services Task Force recommendation Statement. JAMA 2018; 319(24):2521–31. [PubMed: 29946735]

29. Guzon-Illescas O, Perez Fernandez E, Crespí Villarias N, et al. Mortality after osteoporotic hip fracture: incidence, trends, and associated factors. J Orthop Surg Res 2019;14(1):203. [PubMed: 31272470]
30. Menéndez-Colino R, Alarcon T, Gotor P, et al. Baseline and pre-operative 1-year mortality risk factors in a cohort of 509 hip fracture patients consecutively admitted to a co-managed orthogeriatric unit (FONDA Cohort). Injury 2018;49(3): 656–61. [PubMed: 29329713]
31. Ebeling PR, Nguyen HH, Aleksova J, et al. Secondary osteoporosis. Endocr Rev 2022;43(2):240–313. [PubMed: 34476488]
32. Hillier TA, Stone KL, Bauer DC, et al. Evaluating the value of repeat bone mineral density measurement and prediction of fractures in older women: the study of osteoporotic fractures. Arch Intern Med 2007;167(2):155–60. [PubMed: 17242316]
33. Sollmann N, Löffler MT, Kronthaler S, et al. MRI-based quantitative osteoporosis imaging at the spine and femur. J Magn Reson Imaging 2021; 54(1):12–35. [PubMed: 32584496]
34. Black DM, Cauley JA, Wagman R, et al. The ability of a single BMD and fracture history assessment to predict fracture over 25 Years in postmenopausal women: the study of osteoporotic fractures. J Bone Miner Res 2018;33(3):389–95. [PubMed: 28719727]
35. Reilly CC, Raynor WY, Hong AL, et al. Diagnosis and monitoring of osteoporosis with 18F-sodium fluoride PET: an Unavoidable Path for the foreseeable future. Semin Nucl Med 2018;48(6): 535–40. [PubMed: 30322479]
36. Blake GM, Fogelman I. Technical principles of dual energy x-ray absorptiometry. Semin Nucl Med 1997;27(3):210–28. [PubMed: 9224663]
37. Osteoporosis to prevent fractures: screening. Available at: https://www.uspreventiveservicestaskforce.org/uspstf/recommendation/osteoporosis-screening. Accessed May 10, 2022.
38. Damilakis J, Adams JE, Guglielmi G, et al. Radiation exposure in X-ray-based imaging techniques used in osteoporosis. Eur Radiol 2010;20(11): 2707–14. [PubMed: 20559834]
39. Akram S, Chowdhury YS. Radiation exposure of medical imaging. In: StatPearls. StatPearls Publishing; 2021. https://www.ncbi.nlm.nih.gov/pubmed/33351446.
40. Berger A. Bone mineral density scans. BMJ 2002; 325(7362):484. [PubMed: 12202332]
41. Oei L, Koromani F, Rivadeneira F, et al. Quantitative imaging methods in osteoporosis. Quant Imaging Med Surg 2016;6(6):680–98. [PubMed: 28090446]
42. Brett AD, Brown JK. Quantitative computed tomography and opportunistic bone density screening by dual use of computed tomography scans. J Orthop Translat 2015;3(4):178–84. [PubMed: 30035056]
43. Tse JJ, Smith ACJ, Kuczynski MT, et al. Advancements in osteoporosis imaging, screening, and study of disease etiology. Curr Osteoporos Rep 2021;19(5):532–41. [PubMed: 34292468]
44. Michalski AS, Besler BA, Burt LA, et al. Opportunistic CT screening predicts individuals at risk of major osteoporotic fracture. Osteoporos Int 2021; 32(8):1639–49. [PubMed: 33566138]
45. Adams AL, Fischer H, Kopperdahl DL, et al. Osteoporosis and hip fracture risk from routine computed tomography scans: the fracture, osteoporosis, and CT Utilization study (FOCUS). J Bone Miner Res 2018;33(7):1291–301. [PubMed: 29665068]
46. Koch V, Hokamp NG, Albrecht MH, et al. Accuracy and precision of volumetric bone mineral density assessment using dual-source dual-energy versus quantitative CT: a phantom study. Eur Radiol Exp 2021;5(1):43. [PubMed: 34608576]
47. Gruenewald LD, Koch V, Martin SS, et al. Diagnostic accuracy of quantitative dual-energy CT-based volumetric bone mineral density assessment for the prediction of osteoporosis-associated fractures. Eur Radiol 2022;32(5):3076–84. [PubMed: 34713330]
48. Wichmann JL, Booz C, Wesarg S, et al. Dual-energy CT-based phantomless in vivo three-dimensional bone mineral density assessment of the lumbar spine. Radiology 2014;271(3):778–84. [PubMed: 24475863]
49. Blake GM, Puri T, Siddique M, et al. Site specific measurements of bone formation using [18F] sodium fluoride PET/CT. Quant Imaging Med Surg 2018;8(1):47–59. [PubMed: 29541623]
50. Blau M, Nagler W, Bender MA. Fluorine-18: a new isotope for bone scanning. J Nucl Med 1962;3: 332–4. Available at: https://www.ncbi.nlm.nih.gov/pubmed/13869926. [PubMed: 13869926]

51. Raynor W, Houshmand S, Gholami S, et al. Evolving role of molecular imaging with 18F-sodium fluoride PET as a biomarker for calcium metabolism. Curr Osteoporos Rep 2016;14(4): 115–25. [PubMed: 27301549]
52. Blake GM, Siddique M, Frost ML, et al. Imaging of site specific bone turnover in osteoporosis using positron emission tomography. Curr Osteoporos Rep 2014;12(4):475–85. [PubMed: 25168931]
53. Park PSU, Raynor WY, Sun Y, et al. 18F-Sodium fluoride PET as a diagnostic modality for metabolic, Autoimmune, and osteogenic bone disorders: cellular mechanisms and clinical applications. Int J Mol Sci 2021;22(12). 10.3390/ijms22126504.
54. Zhang V, Koa B, Borja AJ, et al. Diagnosis and monitoring of osteoporosis with total-body 18F-sodium fluoride-PET/CT. PET Clin 2020;15(4):487–96. [PubMed: 32768370]
55. Haim S, Zakavi R, Imamovic L, et al. Predictive Value of 18F-NaF PET/CT in the Assessment of Osteoporosis: Comparison with Dual-Energy X-Ray Absorptiometry (DXA). European Journal of Nuclear Medicine and Molecular Imaging 2017;44:S857.
56. Dyrberg E, Larsen EL, Hendel HW, et al. Diagnostic bone imaging in patients with prostate cancer: patient experience and acceptance of NaF-PET/CT, choline-PET/CT, whole-body MRI, and bone SPECT/CT. Acta Radiol 2018;59(9):1119–25. [PubMed: 29313360]
57. Velez EM, Desai B, Jadvar H. Treatment response assessment of skeletal metastases in prostate cancer with 18F-NaF PET/CT. Nucl Med Mol Imaging 2019;53(4):247–52. [PubMed: 31456857]
58. Moore AEB, Blake GM, Fogelman I. Quantitative measurements of bone remodeling using 99mTc-methylene diphosphonate bone scans and blood sampling. J Nucl Med 2008;49(3):375–82. [PubMed: 18287266]
59. Wale DJ, Wong KK, Savas H, et al. Extraosseous findings on bone Scintigraphy using fusion SPECT/CT and correlative imaging. AJR Am J Roentgenol 2015;205(1):160–72. [PubMed: 26102395]
60. Blake GM, Frost ML, Moore AEB, et al. The assessment of regional skeletal metabolism: studies of osteoporosis treatments using quantitative radionuclide imaging. J Clin Densitom 2011;14(3):263–71. [PubMed: 21600822]
61. Ahuja K, Sotoudeh H, Galgano SJ, et al. 18F-Sodium fluoride PET: history, technical feasibility, mechanism of action, normal biodistribution, and diagnostic performance in bone metastasis detection compared with other imaging modalities. J Nucl Med Technol 2020;48(1):9–16. [PubMed: 31811067]
62. Blake GM, Siddique M, Frost ML, et al. Radionuclide studies of bone metabolism: do bone uptake and bone plasma clearance provide equivalent measurements of bone turnover? Bone 2011; 49(3):537–42. [PubMed: 21689803]
63. Frost ML, Moore AE, Siddique M, et al. $^{18}$F-fluoride PET as a noninvasive imaging biomarker for determining treatment efficacy of bone active agents at the hip: a prospective, randomized, controlled clinical study. J Bone Miner Res 2013;28(6): 1337–47. [PubMed: 23322666]
64. Huang SCH. Pharmacokinetic modeling. Mol Imaging 2021;1625–31.
65. Carson RE. Tracer kinetic modeling in PET. In: Bailey DL, Townsend DW, Valk PE, et al., editors. Positron emission tomography: basic sciences. London: Springer; 2005. p. 127–59.
66. Puri T, Frost ML, Cook GJ, et al. [18F] sodium fluoride PET kinetic parameters in bone imaging. Tomography 2021;7(4):843–54. [PubMed: 34941643]
67. Hawkins RA, Choi Y, Huang SC, et al. Evaluation of the skeletal kinetics of fluorine-18-fluoride ion with PET. J Nucl Med 1992;33(5):633–42. Available at: https://www.ncbi.nlm.nih.gov/pubmed/1569473. [PubMed: 1569473]
68. Piert M, Zittel TT, Machulla HJ, et al. Blood flow measurements with [(15)O]H2O and [18F]fluoride ion PET in porcine vertebrae. J Bone Miner Res 1998;13(8):1328–36. [PubMed: 9718202]
69. Griffith JF, Yeung DKW, Tsang PH, et al. Compromised bone marrow perfusion in osteoporosis. J Bone Miner Res 2008;23(7):1068–75. [PubMed: 18302498]
70. Prisby RD, Ramsey MW, Behnke BJ, et al. Aging reduces skeletal blood flow, endothelium-dependent vasodilation, and NO bioavailability in rats. J Bone Miner Res 2007;22(8):1280–8. [PubMed: 17451371]

71. Reeve J, Arlot M, Wootton R, et al. Skeletal blood flow, iliac histomorphometry, and strontium kinetics in osteoporosis: a relationship between blood flow and corrected apposition rate. J Clin Endocrinol Metab 1988;66(6):1124–31. [PubMed: 3372678]
72. Cook GJR, Lodge MA, Blake GM, et al. Differences in skeletal kinetics between vertebral and humeral bone measured by 18F-fluoride positron emission tomography in postmenopausal women. J Bone Miner Res 2010;15(4):763–9.
73. Pantel AR, Viswanath V, Muzi M, et al. Principles of tracer kinetic analysis in oncology, Part I: principles and overview of methodology. J Nucl Med 2022; 63(3):342–52. [PubMed: 35232879]
74. Aaltonen L, Koivuviita N, Seppänen M, et al. Correlation between 18F-Sodium Fluoride positron emission tomography and bone histomorphometry in dialysis patients. Bone 2020;134:115267. [PubMed: 32058018]
75. Messa C. Bone metabolic activity measured with positron emission tomography and [18F]fluoride ion in renal osteodystrophy: correlation with bone histomorphometry. J Clin Endocrinol Metab 1993; 77(4):949–55. [PubMed: 8408470]
76. Cook GJR, Blake GM, Marsden PK, et al. Quantification of skeletal kinetic indices in Paget's disease using Dynamic18F-fluoride positron emission tomography. J Bone Miner Res 2002;17(5):854–9. [PubMed: 12009016]
77. Bloomfield SA, Hogan HA, Delp MD. Decreases in bone blood flow and bone material properties in aging Fischer-344 rats. Clin Orthop Relat Res 2002;396:248–57.
78. Vogt MT, Cauley JA, Kuller LH, et al. Bone mineral density and blood flow to the lower extremities: the study of osteoporotic fractures. J Bone Miner Res 1997;12(2):283–9. [PubMed: 9041062]
79. Nzeusseu Bol I. 18F-fluoride PET for monitoring therapeutic response in Paget's disease of bone. J Nucl Med 2005. Available at: https://jnm.snmjournals.org/content/46/10/1650.short.
80. Siddique A, Green T. Is response assessment of breast cancer bone metastases better with measurement of 18F-fluoride metabolic flux than with measurement of 18F-fluoride PET/CT SUV. J Nucl Med 2019. Available at. https://jnm.snmjournals.org/content/60/3/322.short.
81. Patlak CS, Blasberg RG, Fenstermacher JD. Graphical evaluation of blood-to-brain transfer constants from multiple-time uptake data. J Cereb Blood Flow Metab 1983;3(1):1–7. [PubMed: 6822610]
82. Mathavan N, Koopman J, Raina DB, et al. 18F-fluoride as a prognostic indicator of bone regeneration. Acta Biomater 2019;90:403–11. [PubMed: 30965143]
83. Puri T, Frost ML, Curran KM, et al. Differences in regional bone metabolism at the spine and hip: a quantitative study using 18F-fluoride positron emission tomography. Osteoporos Int 2013;24(2):633–9. [PubMed: 22581294]
84. Morris MA, Lopez-Curto JA, Hughes SP, et al. Fluid spaces in canine bone and marrow. Microvasc Res 1982;23(2):188–200. [PubMed: 7099016]
85. Schwartz AV. Marrow fat and bone: review of clinical findings. Front Endocrinol 2015;6:40.
86. Haddock B, Fan AP, Jørgensen NR, et al. Kinetic [18F]-Fluoride of the knee in normal volunteers. Clin Nucl Med 2019;44(5):377–85. [PubMed: 30888996]
87. Assiri R, Knapp K, Fulford J, et al. Correlation of the quantitative methods for the measurement of bone uptake and plasma clearance of 18F-NaF using positron emission tomography. Systematic review and meta-analysis. Eur J Radiol 2022;146:110081. [PubMed: 34911006]
88. Siddique B, Moore F. Quantitative PET imaging using 18F sodium fluoride in the assessment of metabolic bone diseases and the monitoring of their response to therapy. PET Clin 2012. Available at: https://www.pet.theclinics.com/article/S1556-8598(12)00060-0/abstract.
89. Vrist MH, Bech JN, Lauridsen TG, et al. Comparison of [18F] NaF PET/CT dynamic analysis methods and a static analysis method including derivation of a semi-population input function for site-specific measurements of bone formation in a population with chronic kidney disease-mineral and bone disorder. EJNMMI Res 2021;11(1):117. [PubMed: 34807325]
90. Karakatsanis NA, Zhou Y, Lodge MA, et al. Generalized whole-body Patlak parametric imaging for enhanced quantification in clinical PET. Phys Med Biol 2015;60(22):8643–73. [PubMed: 26509251]

91. Siddique M, Frost ML, Blake GM, et al. The precision and sensitivity of 18F-fluoride PET for measuring regional bone metabolism: a comparison of quantification methods. J Nucl Med 2011;52(11):1748–55. [PubMed: 21990579]
92. Kurata S, Shizukuishi K, Tateishi U, et al. Age-related changes in pre- and postmenopausal women investigated with 18F-fluoride PET–a preliminary study. Skeletal Radiol 2012;41(8):947–53. [PubMed: 22075716]
93. Ayubcha C, Zirakchian Zadeh M, Stochkendahl MJ, et al. Quantitative evaluation of normal spinal osseous metabolism with 18F-NaF PET/CT. Nucl Med Commun 2018;39(10):945–50. [PubMed: 30086077]
94. Frost ML, Cook GJR, Blake GM, et al. A prospective study of risedronate on regional bone metabolism and blood flow at the lumbar spine measured by 18F-fluoride positron emission tomography. J Bone Miner Res 2003;18(12): 2215–22. [PubMed: 14672357]
95. Gnanasegaran G, Moore AE, Blake GM, et al. Atypical Paget's disease with quantitative assessment of tracer kinetics. Clin Nucl Med 2007;32(10): 765–9. [PubMed: 17885354]
96. Rhodes S, Batzdorf A, Sorci O, et al. Assessment of femoral neck bone metabolism using 18F-sodium fluoride PET/CT imaging. Bone 2020;136: 115351. [PubMed: 32276154]
97. Garnero P, Sornay-Rendu E, Chapuy MC, et al. Increased bone turnover in late postmenopausal women is a major determinant of osteoporosis. J Bone Miner Res 1996;11(3):337–49. [PubMed: 8852944]
98. Clarke B. Normal bone anatomy and physiology. Clin J Am Soc Nephrol 2008;3(Suppl 3):S131–9. [PubMed: 18988698]
99. Ceylan B, Özerdoğan N. Factors affecting age of onset of menopause and determination of quality of life in menopause. Turk J Obstet Gynecol 2015;12(1):43–9. [PubMed: 28913040]
100. Siris ES, Chen YT, Abbott TA, et al. Bone mineral density thresholds for pharmacological intervention to prevent fractures. Arch Intern Med 2004; 164(10):1108–12. [PubMed: 15159268]
101. Stone KL, Seeley DG, Lui LY, et al. BMD at multiple sites and risk of fracture of multiple types: long-term results from the Study of Osteoporotic Fractures. J Bone Miner Res 2003;18(11): 1947–54. [PubMed: 14606506]
102. Marshall D, Johnell O, Wedel H. Meta-analysis of how well measures of bone mineral density predict occurrence of osteoporotic fractures. BMJ 1996; 312(7041):1254–9. [PubMed: 8634613]
103. Cranney A, Jamal SA, Tsang JF, et al. Low bone mineral density and fracture burden in postmenopausal women. CMAJ 2007;177(6):575–80. [PubMed: 17846439]
104. Akkawi I, Zmerly H. Osteoporosis: Curr Concepts. Joints 2018;6(2):122–7. [PubMed: 30051110]
105. Shetty S, Kapoor N, Bondu JD, et al. Bone turnover markers: emerging tool in the management of osteoporosis. Indian J Endocrinol Metab 2016;20(6): 846–52. [PubMed: 27867890]
106. Heaney RP. Is the paradigm shifting? Bone 2003; 33(4):457–65. [PubMed: 14555248]
107. Garnero P, Hausherr E, Chapuy MC, et al. Markers of bone resorption predict hip fracture in elderly women: the EPIDOS Prospective Study. J Bone Miner Res 1996;11(10):1531–8. [PubMed: 8889854]
108. Szulc P, Montella A, Delmas PD. High bone turnover is associated with acceated bone loss but not with increased fracture risk in men aged 50 and over: the prospective MINOS study. Ann Rheum Dis 2008;67(9):1249–55. [PubMed: 18065499]
109. Brazier Grados, Mathieu Kamel. Prediction of bone mass density variation by bone remodeling markers in postmenopausal women with vitamin D insufficiency treated with calcium and vitamin D. J Clin Endocrinol Metab 2003;88(11):5175–9. Available at: https://academic.oup.com/jcem/article-abstract/88/11/5175/2656398. [PubMed: 14602746]
110. Messa C, Goodman WG, Hoh CK, et al. Bone metabolic activity measured with positron emission tomography and [18F]fluoride ion in renal osteodystrophy: correlation with bone histomorphometry. J Clin Endocrinol Metab 1993;77(4):949–55. [PubMed: 8408470]
111. Piert M, Zittel TT, Becker GA, et al. Assessment of porcine bone metabolism by dynamic. J Nucl Med 2001;42(7):1091–100. Available at: https://www.ncbi.nlm.nih.gov/pubmed/11438633. [PubMed: 11438633]
112. Deal CL. Using bone densitometry to monitor therapy in treating osteoporosis: pros and cons. Curr Rheumatol Rep 2001;3(3):233–9. [PubMed: 11352792]

113. Muncie HL Jr, LeBlanc LL. Monitoring osteoporosis treatment: DXA should not be routinely repeated. Am Fam Physician 2010;82(7):749–54. Available at: https://www.ncbi.nlm.nih.gov/pubmed/20879697.

114. Uchida K, Nakajima H, Miyazaki T, et al. Effects of alendronate on bone metabolism in glucocorticoid-induced osteoporosis measured by 18F-fluoride PET: a prospective study. J Nucl Med 2009; 50(11):1808–14. [PubMed: 19837766]

115. Frost ML, Siddique M, Blake GM, et al. Regional bone metabolism at the lumbar spine and hip following discontinuation of alendronate and risedronate treatment in postmenopausal women. Osteoporos Int 2012;23(8):2107–16. [PubMed: 21983795]

116. Borggrefe J, Graeff C, Nickelsen TN, et al. Quantitative computed tomographic assessment of the effects of 24 months of teriparatide treatment on 3D femoral neck bone distribution, geometry, and bone strength: results from the EUROFORS study. J Bone Miner Res 2010;25(3):472–81. [PubMed: 19778182]

117. Sato M, Westmore M, Ma YL, et al. Teriparatide [PTH(1–34)] strengthens the proximal femur of ovariectomized nonhuman primates despite increasing porosity. J Bone Miner Res 2004;19(4): 623–9. [PubMed: 15005850]

118. Black DM, Greenspan SL, Ensrud KE, et al. The effects of parathyroid hormone and alendronate alone or in combination in postmenopausal osteoporosis. N Engl J Med 2003;349(13):1207–15. [PubMed: 14500804]

119. Shi N, Foley K, Lenhart G, et al. Direct healthcare costs of hip, vertebral, and non-hip, non-vertebral fractures. Bone 2009;45(6):1084–90. [PubMed: 19664735]

## KEY POINTS

- While measuring bone mineral content via dual-energy x-ray absorptiometry (DXA) and other modalities has proven useful in clinical management of osteoporosis, these modalities largely miss the complex biology that describe the pathophysiology of osteoporosis.
- The fluoride ion of $^{18}$F-NaF exchanges for a hydroxyl group of hydroxyapatite, making $^{18}$F-NaF PET/computed tomography (CT) a useful tool to measure newly synthesized bone mineral and offers a 3D view of bone metabolism.
- Several methods exist for utilizing $^{18}$F-NaF PET/CT scans, with each their own advantages, limitations, and challenges.
- Dynamic scans and kinetic modeling offer a more robust measurement of bone metabolism and provide estimates of bone perfusion and bone extracellular volume that can help characterize bone health.
- Despite current challenges, $^{18}$F-NaF PET/CT has already demonstrated to be a sensitive readout for response to osteoporosis treatment, as well as significantly correlated with more invasive measures of bone turnover.

## CLINICS CARE POINTS

- Osteoporosis is the most common metabolic bone disorder that is characterized by a disintegration of bone microarchitecture, predisposing individuals to devastating fractures followed by severe loss of quality of life.
- While a diagnosis of osteoporosis can be made by a bone mineral density reading, the underlying cause of this structural change is extremely complex and diverse, consisting of a myriad of biological factors that tip the scale of bone metabolism to favor resorption.
- Here, we introduce $^{18}$NaF PET/computed tomography as an emerging tool that adds the ability to measure bone metabolism, which has already been shown to monitor response to osteoporosis treatment more sensitively compared to DEXA and other structural modalities.
- With the continual advancement of PET technologies and the application of kinetic modeling in the research setting, 18NaF PET/computed tomography has the potential to provide an in vivo assay for bone turnover and other useful parameters related to osteoporosis pathophysiology, including bone perfusion and extracellular fluid volume
- Taken together, $^{18}$NaF PET/computed tomography may emerge as an invaluable clinical readout for characterizing bone health and allow for more sensitive monitoring and screening for osteoporosis.

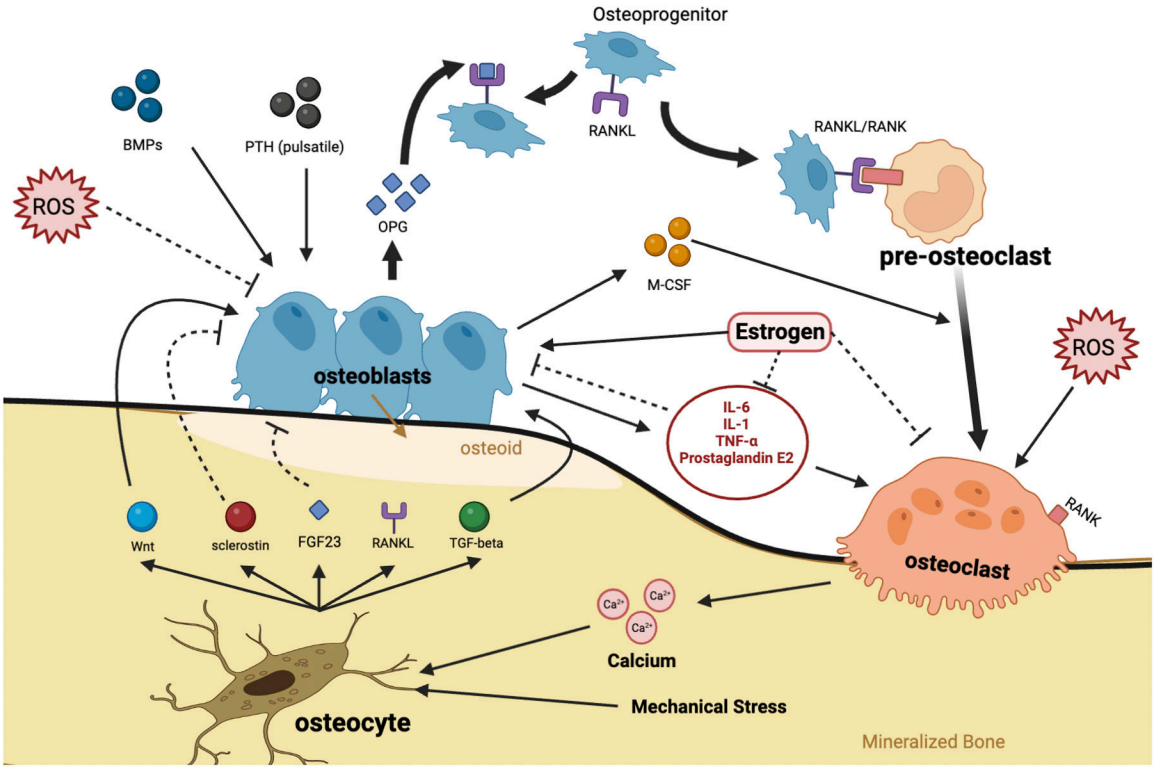


**Fig. 1.**

Bone modeling and remodeling are tightly regulated processes, involving the interactions between osteoblast, osteoclasts, and osteocytes. The molecular interactions illustrated here provide a brief overview of known regulating factors of bone metabolism. For simplicity, osteoblasts can increase osteoclast activity by producing receptor activator of nuclear factor kappa-B ligand (RANKL) and monocyte colony-stimulating factor (M-CSF). Other factors that increase osteoclast resorption include interleukin-1 (IL-1), interleukin-6 (IL-6), tumor necrosis factor-α (TNFα), prostaglandin E2, and reactive oxygen species (ROS). Estrogen leads to a suppression of these inflammatory cytokines and ROS while also directly stimulating osteoblasts and inhibiting osteoclasts. Further, osteoblasts can decrease osteoclast activity by secreting osteoprotegerin (OPG). Factors that increase osteoblast activity include bone morphogenic proteins (BMPs), parathyroid hormone (PTH, pulsatile secretion), transforming growth factor-β (TGF-β), and wingless-related integration site (Wnt) proteins. Osteocytes also receive signals from the environment, mechanical stress, and local calcium to regulate osteoblast and osteoclast function via previously mentioned factors.[5,12–15] FGF23, Fibroblast Growth Factor-23. (Image created with BioRender.com)

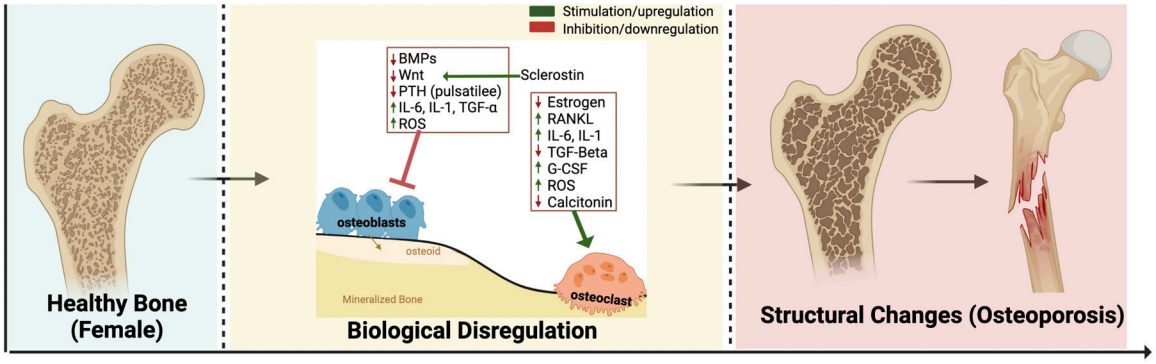


**Fig. 2.**

Early in life, the rate of bone formation exceeds the rate of bone resorption, allowing BMD to peak in the third decade of life (green panel). After this peak, BMD slowly declines with age. In osteoporosis, the decline in BMD is much more pronounced and is preceded by complex biological dysregulation (yellow panel). Many factors have been linked to an increase in osteoclast and decrease in osteoblast activity (green *arrows* signify stimulation or upregulation, and red *arrows* signify inhibition or downregulation, which kick-starts a subsequent decline in bone architecture red panel). (Image created with BioRender.com)

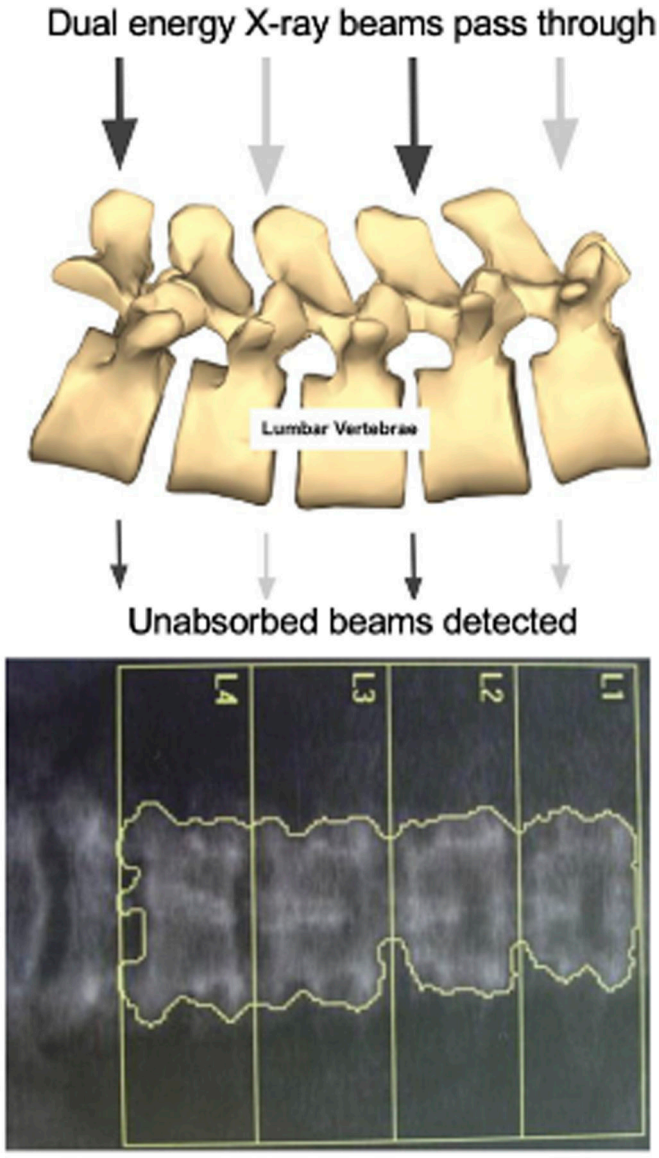


**Fig. 3.**

Diagram of the function of a DXA scan and BMD calculation. Two different X-ray beams, one low-photon and one high-photon energy, are passed through a region of interest (commonly the lumbar spine) to create a pixel-by-pixel map of BMD. The cumulative BMD is then multiplied by the area for that region to get the Bone Mineral Content (BMC).[36] (*Adapted from* Berger A. Bone mineral density scans40. BMJ. 2002 Aug 31;325(7362):484.)

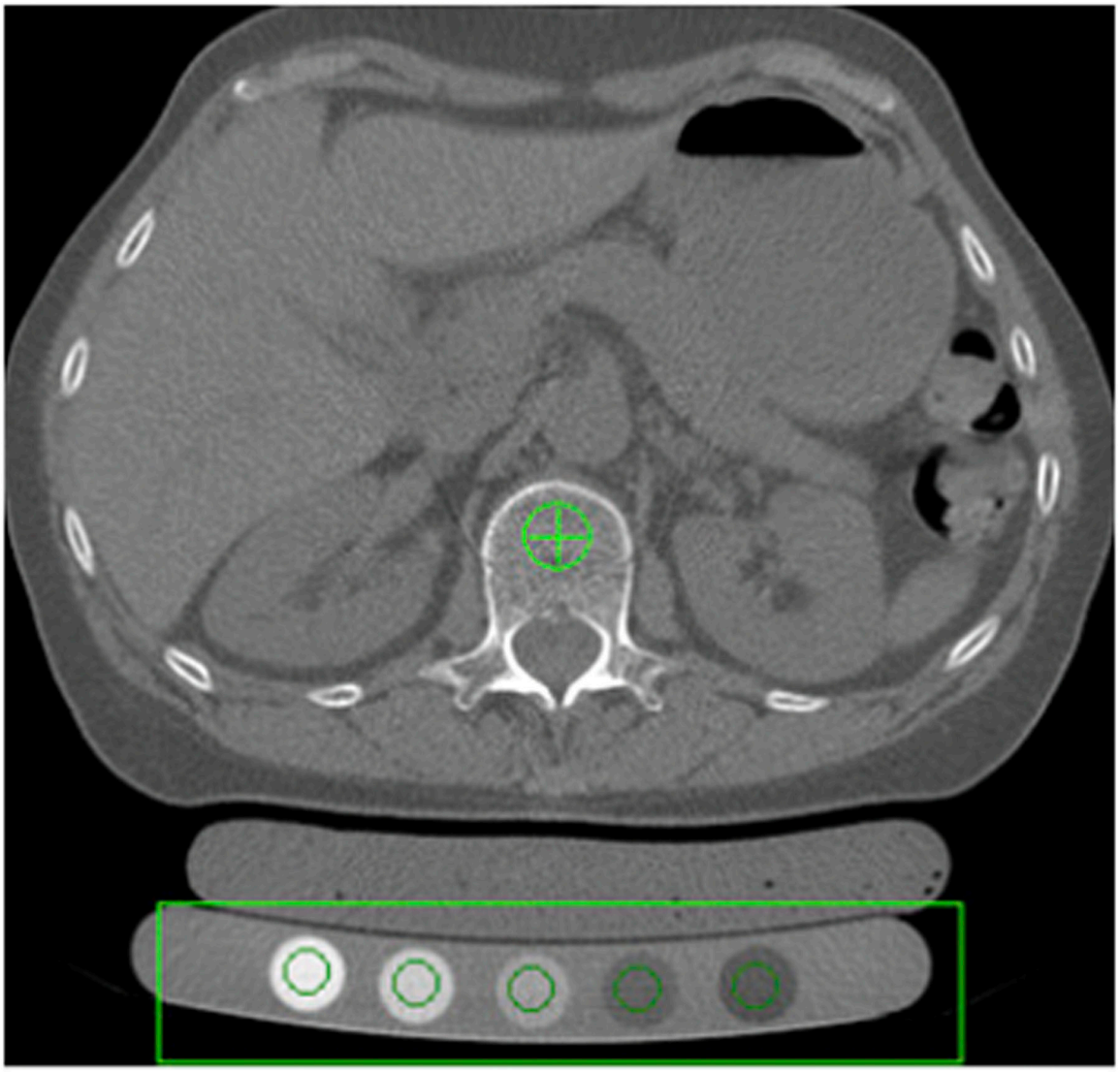

**Fig. 4.**

Cross-section of human subject undergoing qCT of a lumbar vertebrae with a phantom (outlined by green rectangle) for calibration of Hounsfield units (HU) to bone mineral. Illustrated here with permission from Brett and colleagues[42] is a Cann–Genant phantom, which consists of five various concentrations of potassium phosphate-equivalent phases. Once calibrated to the phantom, the HU measurements can be used to estimate bone mineral content within a region of interest (lumbar spine here). From BrettAD, Brown JK. Quantitative computed tomography and opportunistic bone density screening by dual use of computed tomography scans. J Orthop Translat. 2015 Sep 15;3(4):178–184.

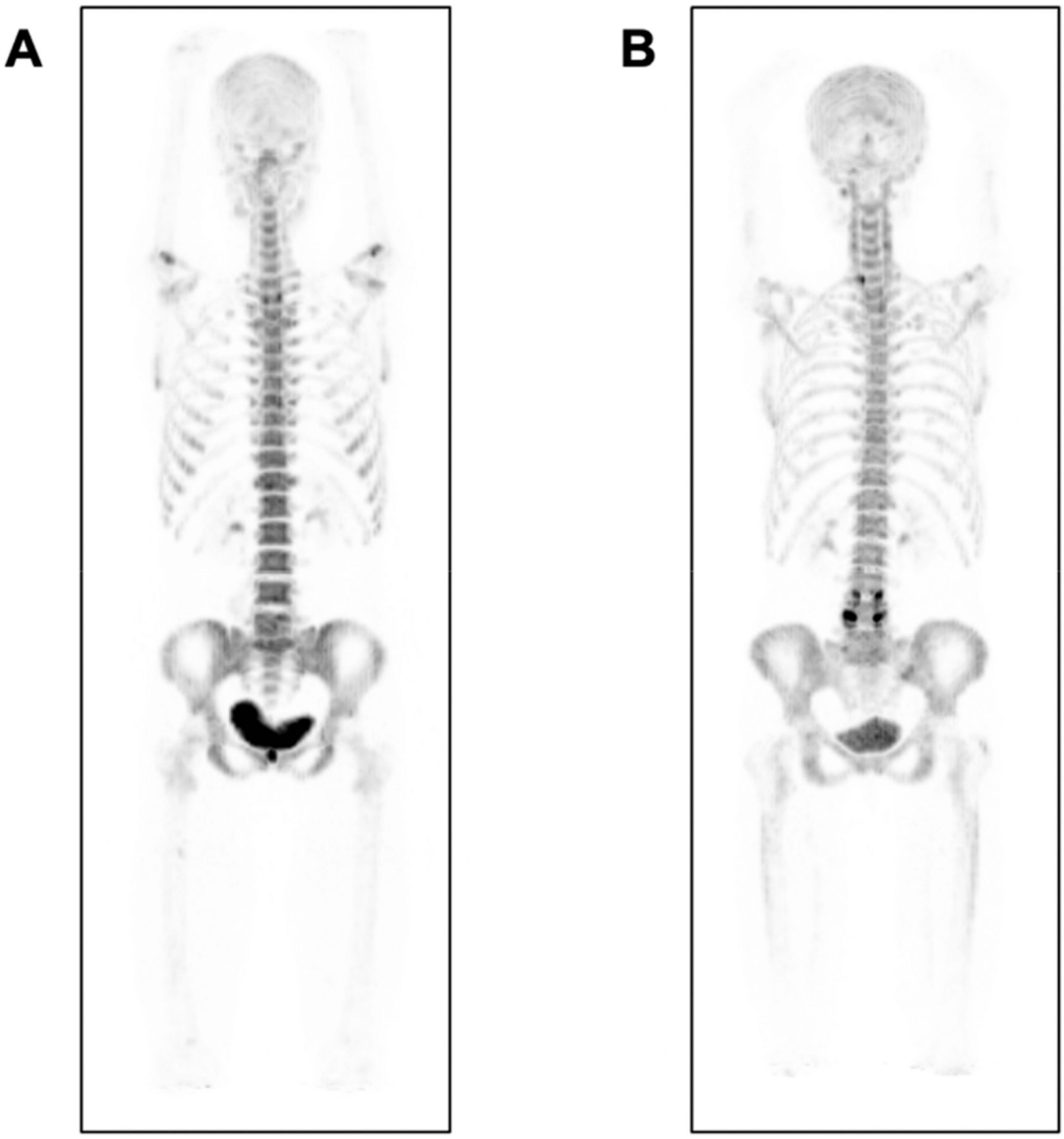


**Fig. 5.**

(*A*) Is a maximum intensity projection (MIP) of a $^{18}$F-NaF scan taken of a healthy 26-year-old woman with normal distribution of radiotracer throughout the skeleton. Although (*B*) is a scan of a 62-year-old woman, showing visible less $^{18}$F-NaF incorporation at the lumbar spine and total hip, indicating the potential of $^{18}$F-NaF PET to detect low levels of bone mineralization. (*From* Park PSU, Raynor WY, Sun Y, Werner TJ, Rajapakse CS, Alavi A. 18F-Sodium Fluoride PET as a Diagnostic Modality for Metabolic, Autoimmune, and Osteogenic Bone Disorders: Cellular Mechanisms and Clinical Applications. Int J Mol Sci. 2021;22(12).)[53]

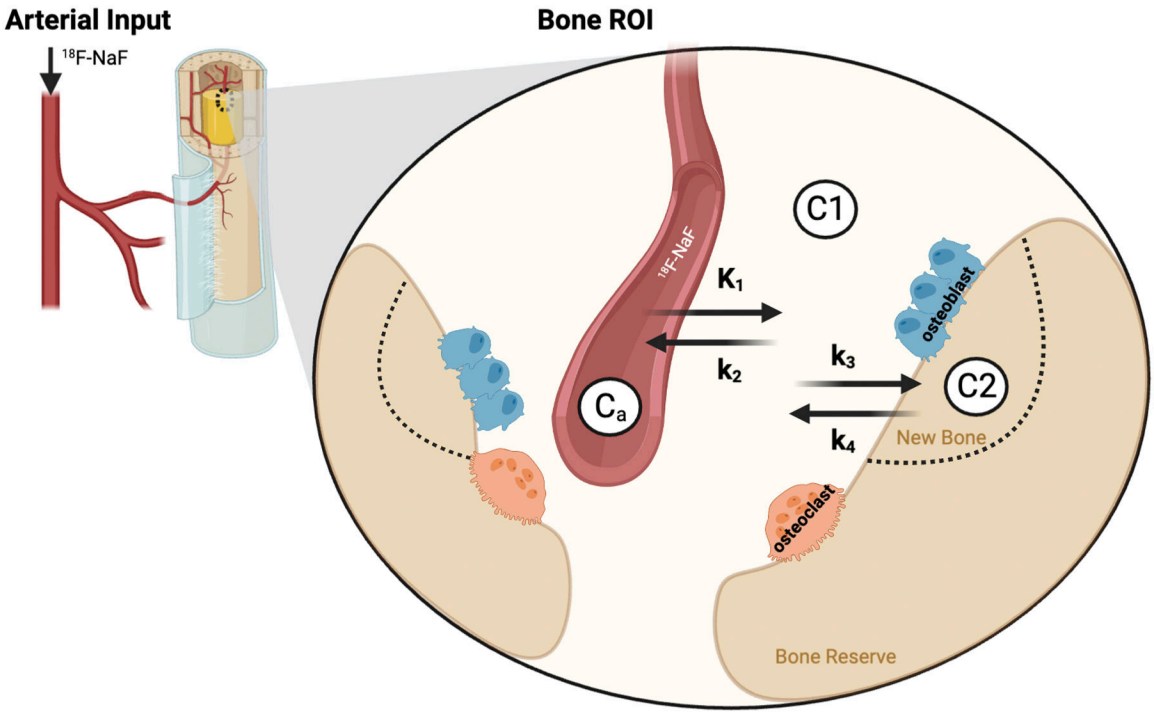


**Fig. 6.**

$^{18}$F-NaF is exchanged from the arterial compartment (labeled $C_a$) into an unbound extracellular compartment (ECF) (labeled C1). The $^{18}$F-NaF within the unbound ECF is also exchanged between the newly mineralized bone compartment (labeled C2), which depends on the amount of new bone mineral available for incorporation of $^{18}$F-NaF. $K_1$ describes the rate of transfer of radiotracer from arterial compartment to the ECF, with units of mL $min^{-1} \cdot cm^{-3}$. $k_2$, $k_3$, and $k_4$ are the rate of transfer of radiotracer from ECF to the arterial compartment, from the ECF to the new bone mineral, and from the bone mineral back into the ECF space, respectively. (Image created with BioRender.com). Park, P.S.U.; Raynor, W.Y.; Sun, Y.; Werner, T.J.; Rajapakse, C.S.; Alavi, A. 18F-Sodium Fluoride PET as a Diagnostic Modality for Metabolic, Autoimmune, and Osteogenic Bone Disorders: Cellular Mechanisms and Clinical Applications. Int. J. Mol. Sci. 2021, 22, 6504. https://doi.org/10.3390/ijms22126504

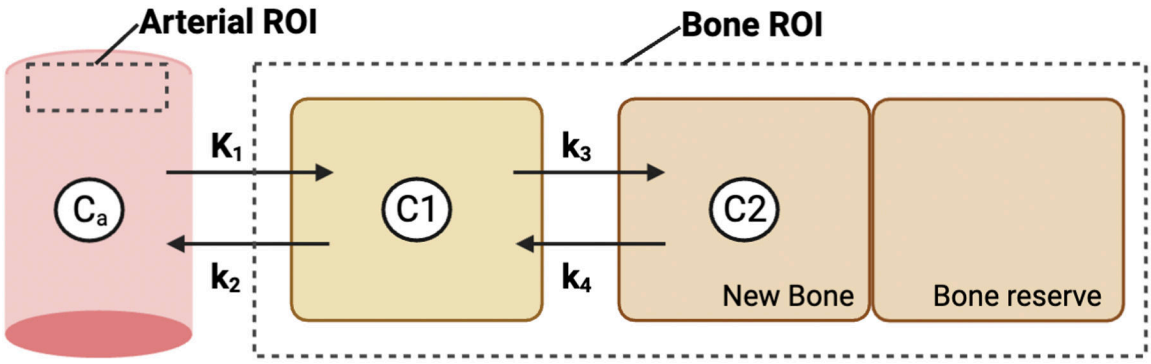


**Fig. 7.**

The two-compartment model of bone (Hawkins model), a simplified schematic of Fig. 7. (Image created with BioRender.com)

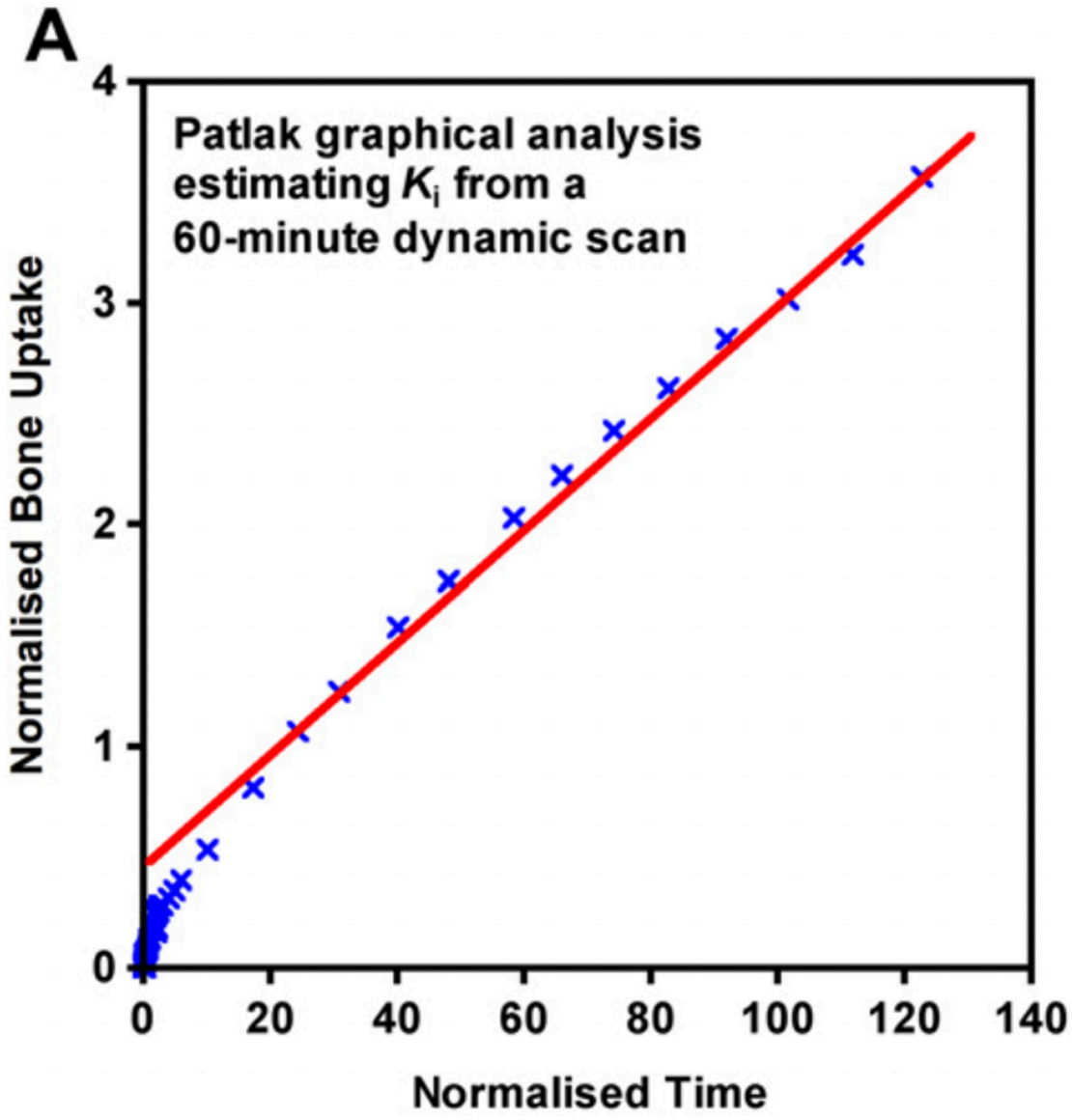


**Fig. 8.**

The Patlak plot (used with permission from Blake and colleagues[88]) represents a graphical approach to solving for $K_i$, which is estimated by plotting the tissue concentration normalized to arterial concentration as a function of normalized time. Normalized time is the integral of the arterial input curve divided by the instantaneous plasma concentration.[81] (*From* Blake GM, Siddique M, Frost ML, Moore AE, Fogelman I. Quantitative PET Imaging Using (18)F Sodium Fluoride in the Assessment of Metabolic Bone Diseases and the Monitoring of Their Response to Therapy. PET Clin. 2012 Jul;7(3):275–91.)

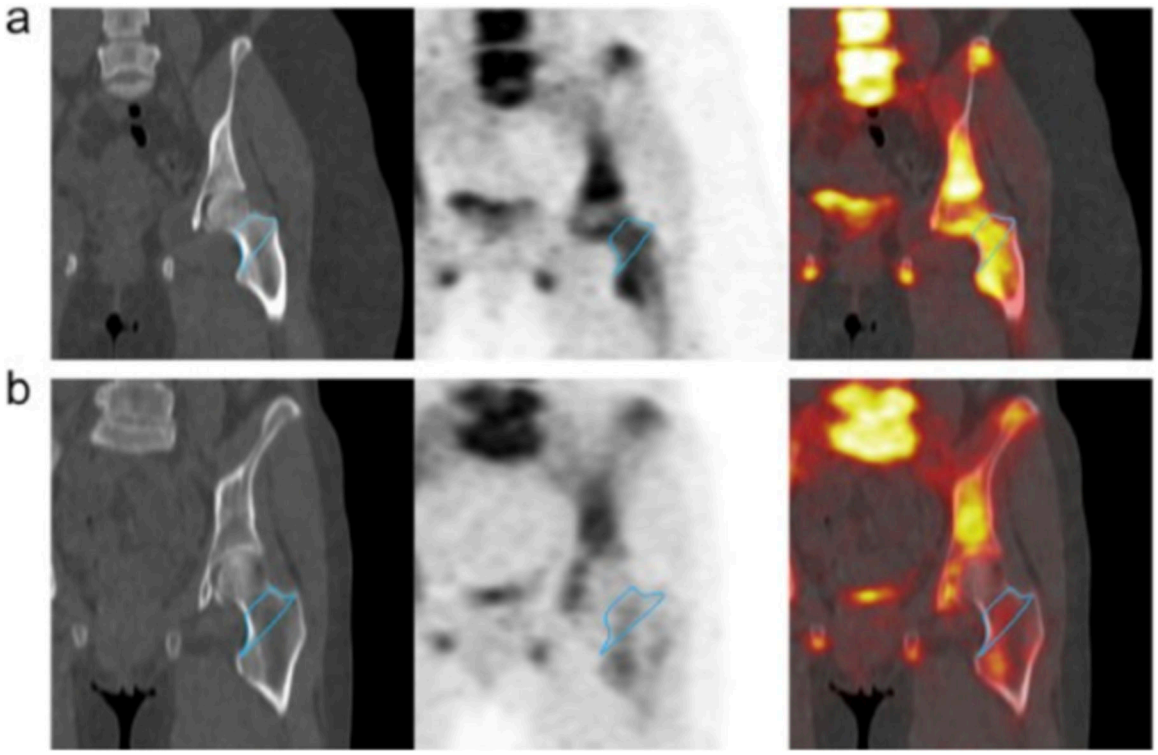


**Fig. 9.**

(*A*) The coronal section of a CT scan (left), static $^{18}$F-NaF PET scan (middle), and a fusion of the two (right) at the left hip of a healthy, 25-year-old woman. (*B*) The same image sequence for a 62-year-old woman. Using the CT image to precisely segment the region of the femoral neck, the amount of radiotracer uptake within that commonly fractured region is easily quantified and can be used to track therapeutic response. (*From* Reilly CC, Raynor WY, Hong AL, et al. Diagnosis and Monitoring of Osteoporosis With 18F-Sodium Fluoride PET: An Unavoidable Path for the Foreseeable Future. *Semin Nucl Med*. 2018;48(6):535–540.)

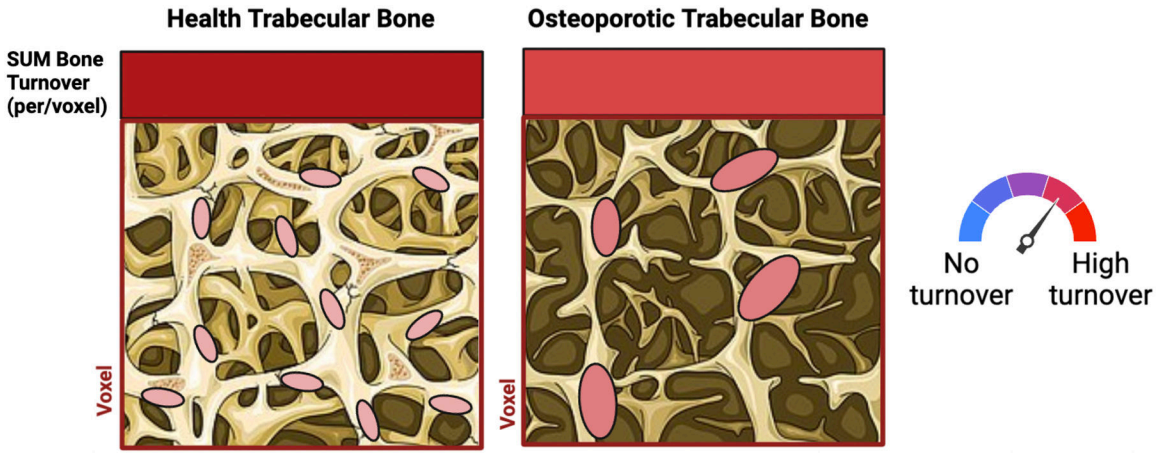


**Fig. 10.**

Red ovals represent bone remodeling units. The greater the intensity of red is, the higher the amount of bone turnover. When capturing $^{18}$F-NaF PET data per voxel, the output SUV is equal to the sum of many bone remodeling units. For osteoporotic bone, with increased bone turnover (per bone remodeling unit), the sum of activity on PET can be less than the sum of activity on PET for healthy bone due to healthy bone having more bone surface area

## Table 1

Kinetic parameters

| Parameter | Units | Functional Definition | Biological Meaning |
|---|---|---|---|
| $K_1$ | $mL/\text{min} \cdot cm^3$ | Volume of $^{18}$F-NaF cleared from plasma pool to ECF space per unit time per unit tissue volume [1] | Given extraction efficiency of $^{18}$F-NaF is near 100% and is not bound to plasma proteins, $K_1$ is closely related to bone blood flow (bone perfusion) [1,2] |
| | | | *Clinical Relevance/example*: Low bone perfusion is significantly correlated with increased bone loss and increased fracture risk [3,4,5] |
| $k_2$ | $1/min$ | Rate of transfer of $^{18}$F-NaF from the ECF space back to arterial compartment [1] | Measure of how efficiently $^{18}$F-NaF moves back to the ECF space. *Potentially* reflects bone microarchitecture and capillary permeability |
| | | | *Clinical Relevance/example*: *Unclear*. Some speculate that can give insight into bone morphology (more trabecular crowding in Paget's disease → more difficult for $^{18}$F-NaF to exchange into arterial compartment) [6]. It may also correlate with capillary permeability [7]. A decrease in $k_2$ may also reflect $^{18}$F-NaF trapped within cells of ECF space ($F^- \rightarrow HF \rightarrow$ diffuses though cell membranes) [1,6] |
| $k_3$ | $1/min$ | Rate of transfer of $^{18}$F-NaF from the ECF space to newly mineralized bone compartment [1] | Direct reflection of mineralization rate and osteoblast activity. Also is an indirect measure of osteoclast function, since both are intricately coupled. |
| | | | *Clinical Relevance/example*: In study of Teriparatide treatment, only $k_3$ showed significant ↑, suggesting it is a sensitive measure of expected increase in osteoblast activity [1,8] |
| $k_4$ | $1/min$ | Rate of transfer of $^{18}$F-NaF from the newly mineralized bone compartment back to the ECF space [1] | Represents a small fraction of $^{18}$F-NaF that is weakly incorporated into exposed hydroxyapatite. |
| | | | *Clinical Relevance/example*: *Unclear*. Near-zero value. Puri et al. has shown that by neglecting its value, it underestimates $^{18}$F-NaF clearance into bone mineral ($K_i$). [1] |
| $K_i$ | $mL/\text{min} \cdot cm^3$ | Volume of $^{18}$F-NaF cleared from plasma pool to newly mineralized bone per unit time per unit tissue volume, represented as bone perfusion ($K_1$) multiplied by the fraction of $^{18}$F-NaF that incorporates into bone mineral from ECF [1] | Most reported parameter. Referred to as bone metabolic flux and a measure of bone turnover. Directly related to bone perfusion (unlike $k_3$), as well as osteoblast activity. |
| | | | *Clinical Relevance/example*: Significantly corelated with histomorphometry data for bone turnover, such as osteoblast per bone surface, osteoclast per bone surface, bone turnover rate, etc. [9]. Is significantly correlated with increased coupling of osteoblasts and osteoclasts [1]. |
| $K_1/k_2$ | $mL/cm^3$ | Volume of distribution of $^{18}$F-NaF within the ECF compartment per tissue volume [1] | For a skeletal region of interest, it describes the volume that is occupied by ECF space. As trabecular volume ↑'s, $K_1/k_2$ ↓'s [1]. |
| | | | *Clinical Relevance/example*: Incorporates estimate of perfusion ($K_1$) and efficiency of $^{18}$F-NaF to transfer back to arterial compartment ($k_2$) to give measure of how much tracer accumulates in ECF space. Gives insight into bone 3D structure. Bones with greater marrow space (vertebrae) have greater $K_1/k_2$ compared with bones with less marrow space (humerus) [7,10]. |

*Data from* [1],[66] [2],[68] [3],[69] [4],[70] [5],[71] [6],[72] [7],[73] [8],[49] [9],[74,75] [10].[76]